STUDY OF FLOW AND HEAT/MASS TRANSFER IN WATER DESALINATION TOWER

by

Qichao Hu

A Thesis Submitted to the Faculty of the

DEPARTMENT OF AEROSPACE AND MECHANICAL ENGINEERING

In Partial Fulfillment of the Requirements

For the Degree of

MASTER OF SCIENCE

In the Graduate College

THE UNIVERSITY OF ARIZONA

2019

THE UNIVERSITY OF ARIZONA
GRADUATE COLLEGE

As members of the Master's Committee, we certify that we have read the thesis prepared by *Qichao Hu* titled *Study ofcFlow and Heat/Mass Transfer in Water Desalination Tower* and recommend that it be accepted as fulfilling the dissertation requirement for the Master's Degree.

Professor Peiwen Li Date: 8-15-2019

Professor Yitshak Zohar Date: 8/15/2019

Professor Qing Hao Date: 8/15/2019

Final approval and acceptance of this thesis is contingent upon the candidate's submission of the final copies of the thesis to the Graduate College.

I hereby certify that I have read this thesis prepared under my direction and recommend that it be accepted as fulfilling the Master's requirement.

Professor Peiwen Li Date: 8-15-2019
Master's Thesis Committee Chair
Dept. of Aerospace & Mechanical Engineering

ACKNOWLEDGEMENT

I would like to thanks all the support from my professors, family and friends.

For the very first I need to give my gratitude to Dr. Li. Without his sagacious advice, I will not be able to finish my work. The knowledge of his rigorous attitude towards research, wisdom in time organization and patience in tedious work would benefit my entire life.

Second, I would like to thanks Dr. Zohar and Dr. Hao for being the committee members of my defense. Those patience suggestions from them always improve my research scientifically.

Third, I would like to thanks my colleges and friends Xiaoxin Wang and Gurangji Chen, the support they give from both my experiments and after school life enriched my life over the past two years.

At the end, I would like to thanks my parents, who support me from the very first day mentally and fanatically.

TABLE OF CONTENTS

LIST OF FIGURES

LIST OF TABLES

Abstract

The paper presents a concept and basic studies about a solar thermal desalination system to achieve the goal of energy efficient, low maintenance, and low-cost water and salts production, leaving no waste discharge and minimum impact on the environment. The system has three major components integrated: a glass-covered solar thermal collection space, a basin with water for evaporation, and a water vapor condensation chimney. Both clean water and salts can be collected to achieve the efficient use of land for solar energy and the maximum value of water and salt products. A preliminary experimental study has demonstrated the concept of the desalination technology with clean water collected at the solar insolation conditions of Tucson, Arizona. Further study for optimization of the coupling of solar collection area and cooling capacity (or cooling heat transfer area) for water vapor condensation will be carried out in the future. This technology is of great significance and value to the water production at arid areas where solar energy is abundant.

Chapter 1. Introduction

1.1 Water Desalination Technologies

With the growth of the human population and climate change, lack of clean water has become a major issue that has been discussed around the world for many years [1]. As a result, more and more researchers have turned their attention to sea water desalination. Sea water desalination is always one of the most important research topics because only 3% of the water on earth is purified (fresh) and usable. On earth, most of the water has salinity of more than 10000 ppm, and the sea water's salinity, which is a range of 35000-45000 ppm, is even higher. The World Health Organization reported that the highest level of salinity the human body can safely accept is normally 500 ppm. In some situations, this value will rise to 1000 ppm, and if the salinity is higher than 1000 ppm it will begin to cause health problems. [2] Fortunately, it is typical that most arid areas in the world are accompanied by an abundance of solar energy. Therefore, using solar energy to produce clean water through desalination of seawater or recycling and treatment of used/damaged water can dramatically reduce the energy cost for clean water production [3-6].

Solar energy can be harvested and converted into thermal energy or electrical energy for different purposes of energy utilization. The energy conversion efficiency from solar energy to electrical energy is still not sufficiently high and the cost of using solar PV or concentrated solar power technology is expensive. However, converting solar energy into thermal energy is relatively easy to accomplish at low cost. Therefore, directly using solar thermal energy for water treatment has a great advantage.

1.1.1 Multi-Stage Flash Distillation and Multi-Effect Distillation

Multi-stage flash desalination and multi-effect distillation are similar, both of which are organized by multiple stages. Each stage consists of a heat exchanger and a condensate collector. With the heat source on the first stage side, it then creates a temperature profile with reduction from first stage to the last stage. First, the water will flow through a/the cold inlet into the heat exchange, then it starts to warm up. Once it reaches and stays in the brine heater, it will reach the maximum temperature. After the brine heat releases the flow into the first stage, since the pressure is lower than the boiling point at current flow temperature, the flow starts to boil. Then water vapor will be separated from the saltine water. The hot vapor will be used to provide heat for the cold water flow heat exchanger and create an equilibrium between energy and pressure inside the stage. Once the heat is absorbed by the heat exchanger, vapor will condense into water and be collected by the collector.

1.1.2 Membrane Desalination

Membrane distillation is the process of using a hydrophobic membrane to interdict the saltine water flow. The water molecules need to change from the liquid phase to the vapor phase to cross through the membrane. Once it returns to a normal pressure and temperature, the purified water vapor will condense into liquid.

The advantage of membrane distillation is working under a minimum external energy and minimum expenditure of capital and land for the plant. [7] It is operated by a significantly lower temperature compared to other conventional distillation systems and results in that the energy required to operate it becomes lower. At the same time, the membrane distillation system employs a hydrophobic microporous membrane to support the vapor-liquid interface, which means its volume is extremely small compared to other conventional distillation systems.

1.1.3 Solar Distillation System

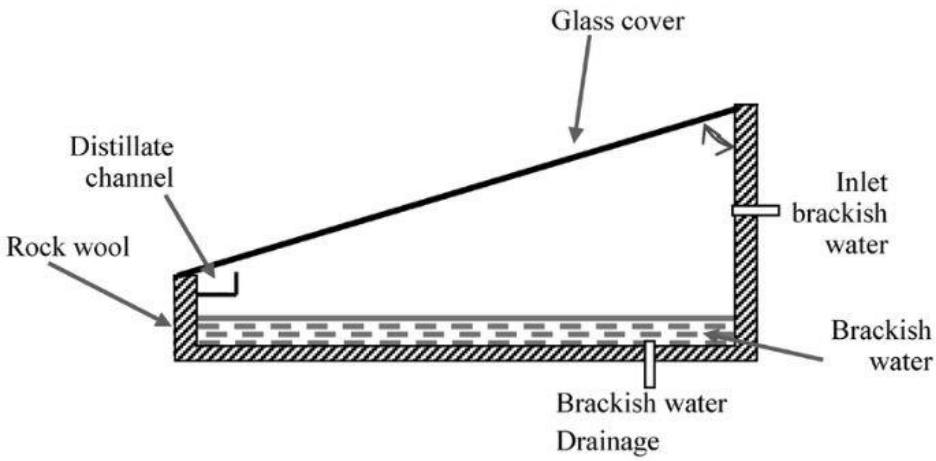

Fig 1. Passive solar still [8]

The Solar Distillation System is one of the most popular water purification technologies and essentially creates a small natural hydrologic cycle of evaporation and condensation inside its interior. The Solar Distillation System is also a relative proven technology, it's been studied and developed since last century, and the very original design is so called the passive solar still. The solar still is a box with an inclined glass cover on top, with the sides of it insulated. Impure water will be filled into the still and due to the energy transformation from solar ray to heat, the water will evaporate. With the temperature difference and vapor density lower than air density, the moist air will naturally flow up to the glass cover; this process is known as natural convection. Then, due to the temperature difference, water will condense on the glass cover and flow into the collector along the slope, where contaminates and microbes will be separated, thus resulting in purified water. A passive solar still has many limitations which lead to low evaporation and condensation. When a passive solar still operates, solar irradiation will be transferred into the heat flux and will then provide power for heating up water and water evaporation simultaneously. The result is the water remains a low temperature, thus the evaporation rate stays low. The low evaporation rate will cause low water production, which

is the major drawback of the passive solar still. For finding out how to improve the solar still structure, the general parameters need to be clarified; these include controllable and uncontrollable parameters. The uncontrollable parameters, also known as the environment condition, are factors such as wind speed, solar radiation intensity, ambient relative humidity and ambient temperature. The rest of the parameters are controllable, for instance, glass cover materials, insulation layer materials, depth of water and temperature of water. Researchers trying to improve the evaporation and condensation by adjusting these controllable parameters lead to the birth of the active solar still. Active solar still is the general name of all solar stills applied with extra thermal technologies, in general speaking, active solar stills split into 3 parts: the pre-heated solar still, nocturnal active solar still and high temperature solar still.

The Pre-heated active solar still system is similar to the idea of a cooling tower. Wasted heat coming out of any industries or power plants will be carried out by water, then heated water will either be fed into the water basin directly or transfer heat into water inside the basin by the heat exchanger. This process leads to the system's ability to operate even during bad weather. In order to have a more clear understanding of the system, the pre-heated active solar still can be considered as a cooling tower with a glass cover sealing the outlet of the tower. Below is a pre-heat solar still investigated by Ashok Kumar and Tiwari [9].

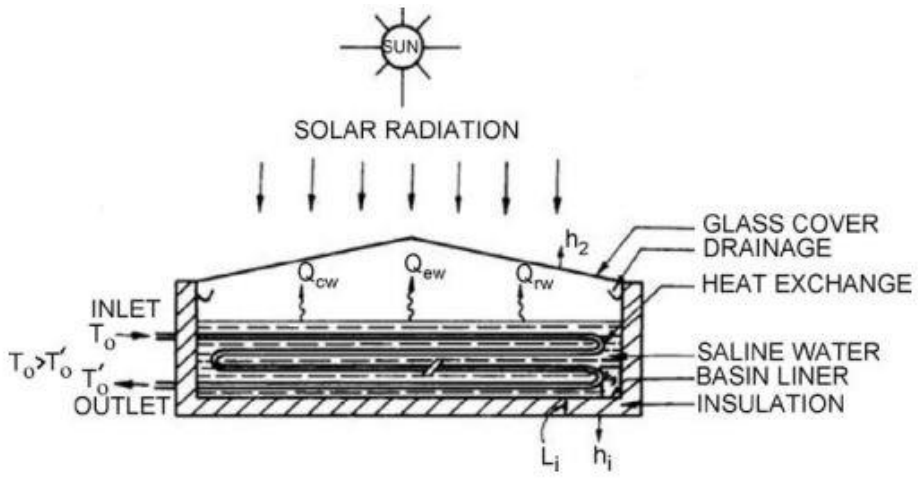

Fig. 2 Schematic diagram of double slope single basin solar still with heat exchanger [9].

Nocturnal active solar still might also be called nocturnal active still. Whether it is a solar still or not is based on whether the energy supplied is sunlight or wasted heat. Similar to the pre-heated water active solar still, energy used to increase and maintain water temperature will be provided by any heat exchanger including the solar collector or feeding hot water into the solar still directly. The difference is its operating nocturnally, with a relatively low ambient temperature and 0 incoming solar energy, the water condensation rate will be higher than day time. Since the still is not operated by solar energy, if the supply heat is not from a solar collector, the nocturnal active still cannot be called as a solar still.

Unlike the previous two active solar still system, the high temperature solar still focuses on how to maximize the use solar energy to improve the performance of the solar still. High temperature solar stills separate the water heating process out of the solar still by using solar collectors such as the solar water heaters shown in Fig 3, heated water will then be fed into the basin of the solar still. From statistical data, the water temperature will increase from 20-50°C to 70-80°C, which will significantly increase the water generation. [10]

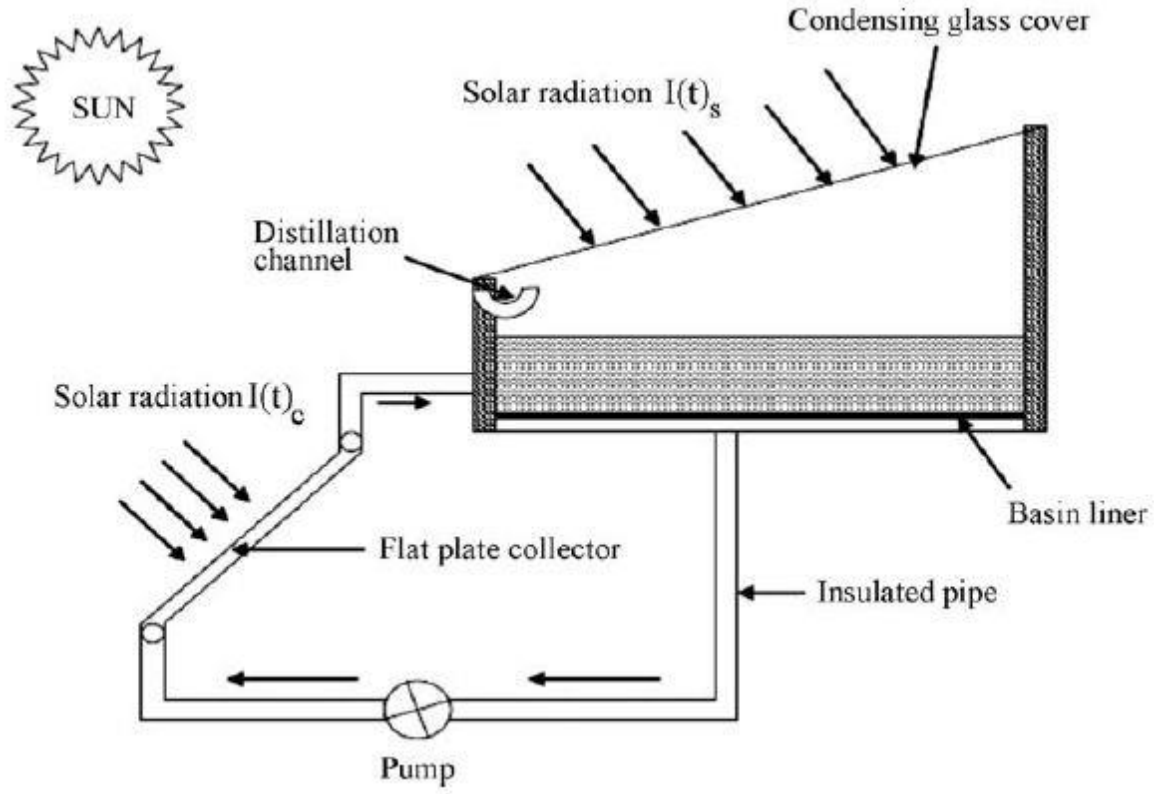

Fig. 3 Schematic of an active solar still integrated with a flat plate collector [11]

1.2 The Proposed New Technology: Water Desalination Tower/Chimney Using Solar Energy

Fig 4 illustrates the novel concept of solar collection and seawater desalination in a glass-covered space. A thin layer of seawater in a water basin is in the glass-covered space, where water evaporates due to the heating from the captured heat from solar energy and the water vapor evaporated from the seawater can rise and be ventilated through a chimney. The chimney is externally cooled by convective ambient air at a relatively lower temperature and also through radiative heat dissipation to the sky. The condensed water at the inner wall of the chimney flows down and is collected by water holders as clean water.

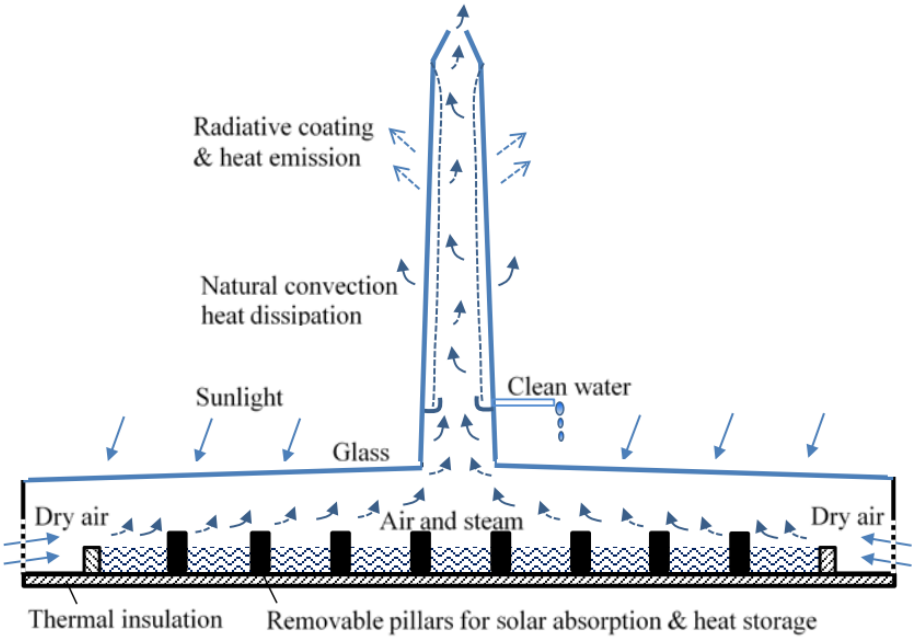

Fig. 4 Concept of glass-covered solar collection and water evaporation basin integrated with cooling chimney for condensation of water vapor for clean water.

The physics involved in the above-described novel solar desalination system include greenhouse effect for solar energy collection, evaporation and condensation heat transfer in phase change processes of water, and flow due to buoyancy effect in the chimney. The glass-covered space is designed to be a space that has black blocks at the bottom of the water basin, which can collect the heat from the sunlight that passes through the glass. The glass material allows the short wave and visible light to go into the space but stops the long wave such as thermal radiation from going out of the solar collection space. This is the greenhouse effect by which solar thermal energy is trapped. The heat absorbed by the black blocks and the black bottom of the water basin provides the energy to cause the water in the glass-covered space to evaporate. This kind of technology is commonly used in the solar distillation system introduced in section 1.1. The main insufficiency of the solar distillation system is the solar energy collection. The condensed water dew causes non-uniform diffusion, reflection, and absorption of the solar irradiation which then reduces solar energy collection.

As a difference, in this new system, water will condense in the chimney section, which means that the condensation of water on the glass is designed to be as little as possible which will thus optimize the solar energy collection. In order to achieve the goal, a design with air flow is used to enhance the convection heat transfer then reduce the water condensation rate on the glass cover's inner surface. As Fig.4 shows, around the shallow water basin, dry air can flow into the glass-covered space due to the pressure difference created by the moist hot air and the chimney effect (buoyancy force). The airflow can carry away the water vapor at the water surface and flow up to the chimney. During this process, mass transfer between water vapor and air occurs from the water surface to the bulk airflow. Similar to the solar distillation system, mass transfer rate or so-called water evaporation rate is based on the convection heat transfer since they happen simultaneously. The difference is, the convection heat transfer in the solar distillation system is natural convection based on temperature difference between the water surface and inner surface of the glass cover. Also, in this new system, the convection heat transfer is based on Poiseuille air flow, which is an enhancement compared to the natural convection heat transfer. As a result, the water evaporation rate is increased. The airflow velocity and flow rate are majorly determined by the pressure difference that is created by the chimney effect. The higher the chimney is, the more airflow may occur, and thus more water vapor can be taken away.

The chimney must be made to have a thermal conductive thin wall in order to better release the heat from the moisture-laden airflow to the ambient air outside of the chimney. At the outside wall of the chimney, natural convective heat transfer between the chimney and ambient air occurs. In the meantime, radiative coating can be applied to the outer surface of the chimney to get more energy to be radiated to the sky, which has a lower temperature than the chimney surface.[12] While the heat transfer coefficient of evaporation and condensation is very effective, the heat transfer from the chimney to the ambient air can be the major thermal

resistance that dominates the clean water collection rate. Therefore, external fins at the outer surface of the chimney might also be adopted for heat transfer enhancement. The condensed water at the inner surface of the chimney can flow down to a water holder. The entire system desalinates seawater by relying on solar energy and natural phenomena of the chimney effect and natural convective air cooling, with addition of radiative cooling. The land utilization for solar collection can reach 100 percent (compared to trough or heliostat solar concentrating technologies) and the system operation does not need electrical power to drive the flows, which thus results in very low cost for operation and maintenance.

Chapter 2. Water desalination tower design and proof of concept

2.1 system layout and design

2.1.1 System layout

A small test unit for the proof-of-concept has been constructed and has two parts, the glass-covered solar collection space and the chimney for the cooling and condensation of water vapor for clean water collection. As shown in Fig. 5, the glass-covered space is a shallow water basin, which is essentially a black plastic pan, with inner and outer diameters of 24/26 inches (0.61m/0.66m). A clear polycarbonate glass with a diameter of 30 inches (0.76m) and a thickness of 0.25 inches (6.4 mm) covers the plastic pan. The gap between the polycarbonate glass cover and the pan can be adjusted by ⅛ inches gaskets for the need of optimization of the gap for maximum water production. There will be a thermocouple step into water near water surface.

In the center of the polycarbonate glass plate, a hole/opening with a diameter of 4 inches (10.2 cm) is connected to the chimney allowing humid air in the solar collection space to ventilate through the chimney. Commercial available copper or aluminum tubes were used for the chimney. Three supporting sticks were employed to hold the weight of the chimney, as shown in Fig. 5.

The chimney outside surface may absorb sunlight to make the chimney hot. Therefore, reflecting sunlight away at the chimney outside surface to avoid heating up is important for the small test unit. The top opening of the chimney can be adjusted and correspondingly changes the flow rate of the air going into the chimney, which may result in different amounts of water collection.

The first chimney tested in this work is made of copper, which is 44 inches (1.12 m) in height, 10.2 cm in inner diameter, and 1.6 mm in thickness. A conic cap covers the top of the

chimney. The cap is 7.62 cm in height, with a top opening diameter of 25.4mm as shown in Fig. 5. At the bottom of the chimney's inner wall, there is a water holder (like the one shown in Fig. 4) in which water condensate flowing down from the chimney wall is collected. Copper being chosen as the material of chimney is based on its remarkable thermal conductivity, however, it's also has low reflectance at short wavelength include visible light wavelength, for avoiding the solar irradiance absorbed by the chimney, we used metallic coating technique. Detail explanation will shows in 2.1.2

There are four pairs of thermocouples located at the height from the bottom of the chimney at 5.1 cm, 43.2 cm, 78.7 cm and 115.6 cm, respectively. Two situations of the external surface of the copper chimney were tested, one has the copper surface as it is, which absorbs sunlight very well, and the other case has aluminum foil attached to reflect sunlight.

Fig. 5 Photograph of the proof-of-concept unit with a copper chimney for preliminary test

A higher aluminum chimney, as shown in Fig. 6, was also made to investigate the effect of height of the chimney on the water production rate, which affects the flow rate of dry air entering the system. The chimney is of the same inner diameter as that shown in Fig. 6, but has

a greater height of 182.9 cm. The wall thickness of the chimney is 3.5 mm. A conic cap with a height of 7.6 cm and a narrowed opening of 2.2 cm can cover the chimney at the top in a similar way as shown in Fig. 6. There are five pairs of thermocouples inserted in the chimney at locations from the bottom at 5.1cm, 48.3cm, 91.4cm, 134.6cm, and 177.8cm, respectively. Supporting legs were used to hold the weight of the chimney and keep it straight. The outer surface of the aluminum chimney is polished for better reflection of sunlight. Similarly, at the bottom of the chimney there is a water holder for clean water collection. It is noted that the proof-of-concept test unit has a rather small solar collection area. The shadow of the chimney can cause a 5% loss of sunlight to the solar collection space. A larger solar collection area will be better for more tests in the future.

Fig. 6 Photograph of the proof-of-concept unit with an aluminum chimney for preliminary test

2.1.2 Design analysis

Chimney area is the most important part of this water desalination project, the water condensation rate is depending on the amount of the heat can be transfer out of the chimney. Therefore choose which material and what kind of structure to make the chimney is very important.

When after considering about wind force load, contact area between moist air flow and chimney inner surface area, the shape of hollow cylinder were chosen. The simulation is shows below:

The deflection of a bar with bottom fixed is equal to

$$Y = \frac{FL^3}{3EI} \tag{1}$$

Where F is the wind force applied horizontally to the ground, L is the height of the chimney, E is Young's modulus and I is the moment of inertia. When 2 chimneys made by same material with same height, the comparison of deflection in between this two chimneys will depends on the moment of inertia, which are

$$I = \frac{\pi}{64}[{d_o}^4 - {d_i}^4] \tag{2}$$

$$I = \frac{1}{12}[BH^3 - bh^3] \tag{3}$$

For same amount of materiel which means at same volume of material, round hollow section will always have higher moment of inertia then rectangle and square hollow section. As a result, cylinder chimney will has less deflection than others. One additional reason to choose cylinder chimney as the shape of the chimney is, it has uniform thickness than any polygon which apply uniform conduction heat transfer.

At the start of the experiment, because of coppers high thermal conductivity (which is 401 W/m*K), it was considered as the material to produce chimney. However, at here metallic reflection wasn't fully considered. All metals have high reflectivity, and that is based on its high damping constant result in short light cross distance. It is necessary to mention that most metal have high reflectance at long wavelength range, but at short wavelength range, metal like copper and gold will have poor reflectance. For instance, from Fig. 7, copper have low reflectance at short wavelength include visible range, which then lead to when white light irradiate on copper appears brown, and it result in high absorptance of copper at short wavelength range, then lead to heat flux flows from outside of the chimney to inside which is

opposite of the design plan. This insufficient consideration effect the first group of experiment shows in section 2.3.

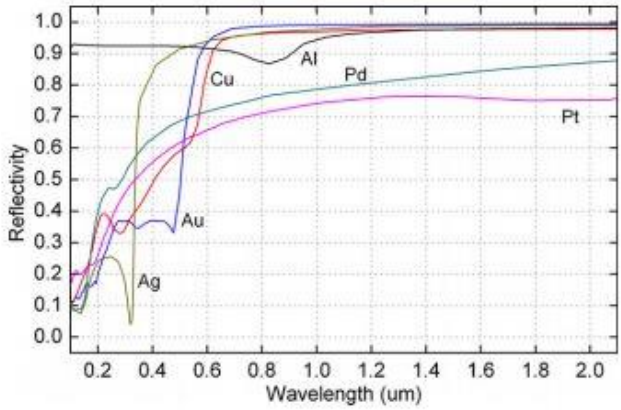

Fig. 7 Reflectivity of metals versus wavelength at normal incidence [13]

For solving the solar irradiation absorption problem, metallic reflection topic are continue studied. Like Fig. 7 shows again, aluminum and sliver are different than copper and gold, they have high reflectance which very close to 1, that cause they are colorless than copper and gold, at the same time, it makes them basically reject all of the solar radiation heat. This metallic property result in metallic coating become a popular technology in nowadays. According to above analysis, we improve the concept by applied the aluminum coating on copper chimney and choose aluminum to be the material of the new chimney.

6061 Aluminum is one of most common aluminum material metal company and fabrication factory can supplied, difference than copper, it has less thermal conductivity which is 167 W/m*K, however, based on its reflectance and cheap price, it is more practical to build a Aluminum chimney tower than a copper chimney tower, that is the reason at the end of this experiment an aluminum chimney was chosen.

2.2 Basic analysis on chimney effect and water production

A fundamental understanding to the ideal water production rate is necessary for evaluating the potential of the technology. Two ideal scenarios may be assumed for the analysis of the desalination system.

The first case is to simply count the evaporation of water based on the energy trapped in the solar collection space. In an enclosed system, the water vapor rises to the chimney and cools down/condenses into liquid water. If the trapped thermal energy is predictable in a certain period of time, the generated clean water can be simply estimated in the form of:

$$Q = \beta \cdot I_{solar} \cdot A \cdot \Delta t \tag{3}$$

$$m_{H2O} = \frac{Q}{r} \tag{4}$$

where I_{solar} is the solar irradiance heat flux (W/m^2), β is the percentage that the energy from the sunlight is trapped inside the solar collection space, A is the area through which sunlight enters the energy collection space, Δt is the time period of operation with sunlight, r is the latent heat of water vaporization.

In the second case of analysis, dry air flows into the glass-covered solar collection space, and the heat and mass transfer between the air and the evaporating water surface fully humidifies the air to reach a humidity of 1.0. The hot humid air is assumed to be fully cooled down in the chimney and liquid water precipitates so that the humidity of air reaches 1.0 at a lower temperature near ambient air. The water precipitation can be calculated based on the high and low temperatures assuming the moisture-laden air is ideal gas.

The pressure of air at the solar collection space inlet is assumed as 1.0 atm, which gives,

$$P_{inlet} = 1.0atm = \rho_{dry-air} g h_{\infty} \tag{5}$$

where $\rho_{dry-air}$ is the dry air density, g is gravity, and h_∞ is the thickness of air covering earth. While at the outlet of the chimney, the pressure of air is calculated as:

$$P_{outlet} = \rho_{dry-air} g\left(h_\infty - h_{chimney}\right) \tag{6}$$

where $h_{chimney}$ is the height of the chimney. The pressure inside the chimney is different, which depends on the humidity of the air, and therefore there is:

$$\rho_{moist-air} = \rho_{dry-air} * \frac{1+x}{1+x*\frac{R_{water}}{R_{air}}} \tag{7}$$

where R_{water} and R_{air} are the gas constants of water and air, respectively; x is the humidity of the air. Then, from the above equations, the pressure at the entrance of chimney is obtained as:

$$P_{bottom} = \rho_{dry-air} g\left(h_\infty - h_{chimney}\right) + \rho_{moist-air} g h_{chimney} \tag{8}$$

After comparing the pressures in Eqs. (5), (6), and (8), there is $P_{inlet} > P_{bottom} > P_{outlet}$, because the density of air (1.2 kg/m^3 at 25 ^{o}C) is larger than the density of the water vapor (0.1302 kg/m^3 heated at 60 ^{o}C). This indicates the chimney effect that dry air can flow into the solar collection space and carry moisture to flow up into the chimney.

Based on the ideal gas law, the condensed water can be calculated theoretically, which gives:

$$m = \left(\frac{P_{bottom}}{T_{bottom}} - \frac{P_{outlet}}{T_{outlet}}\right) * \frac{1}{R_{water}} \quad \text{kg/s for 1.0 m}^3\text{/s of air flowing in} \tag{9}.$$

The system's actual desalination performance can be greatly affected by the solar collection and water vapor condensation, depending on how well the dry air can be humidified and how thoroughly the moisture-laden air is dehumidified. The chimney is responsible for the condensation heat transfer of humid air inside the chimney. With a higher chimney the air flow rate may increase. Better heat dissipation at the outside of the chimney is also very important for the moisture in the humid air to condense into water.

2.3 Preliminary outdoor experimental test

2.3.1 Experiment set up

The proof-of-concept experimental tests were conducted in fully sunny days in Tucson, Arizona. Before doing any tests, the basin was filled with 5-8 liters of water in a depth of less than 3 cm, and the water was warmed up under the sun for up to one hour to reach a temperature typically above 50 ^{o}C. The humid air can then flow up into the chimney and condenses to clean liquid water for collection.

The temperatures of water and humid air inside the chimney were monitored using NI data acquisition system operated using Labview so that the temperature difference at evaporation and condensation processes can be studied.

The following several different conditions of operations were observed in the experiment.

(1) With different opening gaps between the cover glass and the water basin. This gap affects the amount of air entering the solar collection space and thus affects the temperature of humid air as well as the amount of water condensation in the chimney.

(2) With or without additional cooling—the radiative cooling at the outside surface of the chimney. Other than convective heat loss, the radiative heat dissipation at the outside surface of the chimney can also significantly affect the condensation of water in the chimney. The copper chimney's outside surface absorbs solar radiation very well. This absorbed heat can make the chimney hot. To reduce the absorption of sunlight at the outside of the copper surface of chimney, aluminum foil is attached to the surface.

(3) With different heights of the chimney, the overall heat transfer surface area is different and the thermal syphon chimney effect also becomes different, and thus the water collection performance can be different.

(4) Deteriorated glass transparency and sunlight absorption in the solar collection, and any degradation of heat transfer ability of materials can cause deteriorating performance of water collection.

2.3.2 Experiment result

2.3.2.1 The effect of the gap between cover glass and the water basin

In this test, the copper chimney outer surface had aluminum foil attached to reflect sunlight. The gaps between the cover glass and the water basin were set at 1 mm and 3.4 mm respectively to observe the effect on the water collection. At the gap of 1.0 mm water vapor rises and condenses at the cover glass. However, at the gap of 3.4 mm, the amount of air entering into the gap significantly increased, which made the humid air flow out the chimney before the water vapor condensed into liquid. It was observed that when the gap is 3.4 mm, the collected water is much less than that with a gap of 1.0 mm. It is important to find an optimized gap in order to get more water collection, however, the optimal gap is not a simple parameter, but depends on size of solar collection area, the height of chimney, and the heat transfer performance between the chimney and surroundings. Detailed studies will be carried out in the future.

(a) gap=1 mm (b) gap=3.4 mm

Fig. 8 Effect of the gap between cover glass and the water basin

2.3.2.2 The effect of the cooling at the surface of the chimney

It also has been observed that the surface of the copper chimney absorbed sunlight very well and could became sufficiently hot so that water vapor could not condense. Although copper has very good thermal conductivity, however, in this test unit, the chimney absorbs sufficient sunlight making the chimney hard to cool down. Fig. 9 shows the measured temperatures at different locations of the chimney and the water basin. If the copper chimney is not covered by aluminum foil, the temperature at the top and bottom of the chimney is not clearly differentiated as shown in Fig. 9. (a). With the aluminum foil attached to the surface of the chimney, heat dissipation at the chimney became better. The temperature at the water basin is high and it becomes lower along the height of the chimney, which reflects the cooling down of the humid air and liquid water that was collected in this test.

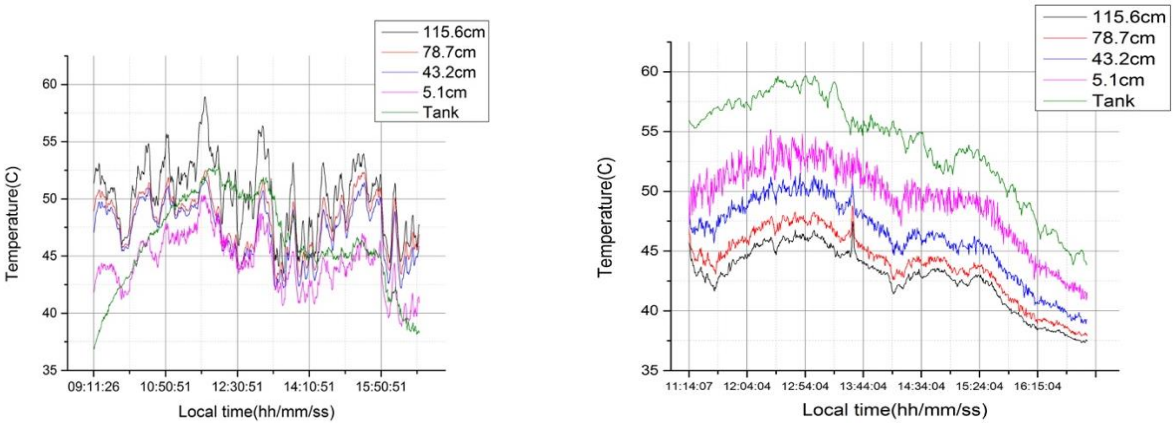

(a) copper chimney surface as it is. (b) copper chimney surface covered with aluminum foil

Fig. 9 Temperature of the air-water vapor mixture inside the chimney along the height.

2.3.2.3 The effect of the opening at the top of the chimney

Due to the limited cooling capability on the outside of the chimney, the flow rate of air in the chimney needs to be properly controlled so that condensation of water vapor can be made possible. When the top opening of the chimney is large, the air flow rate is also large and makes the humid air easily go out and the amount of condensed water is less. With a smaller top opening, the air and water vapor flow rate is smaller and water vapor is easily condensed. Fig. 10 shows the temperature of air and water vapor in the chimney at two days with the same ambient temperature. In the case of smaller top opening, the temperature difference along the chimney is more significant and thus allows for more water collection. Table 1 gives the collected water in different time periods. The case with a smaller top opening could get more water. It was found that the chimney with either a top fully opened or fully closed is not good. This is another proof that optimization of the airflow going into the chimney is important.

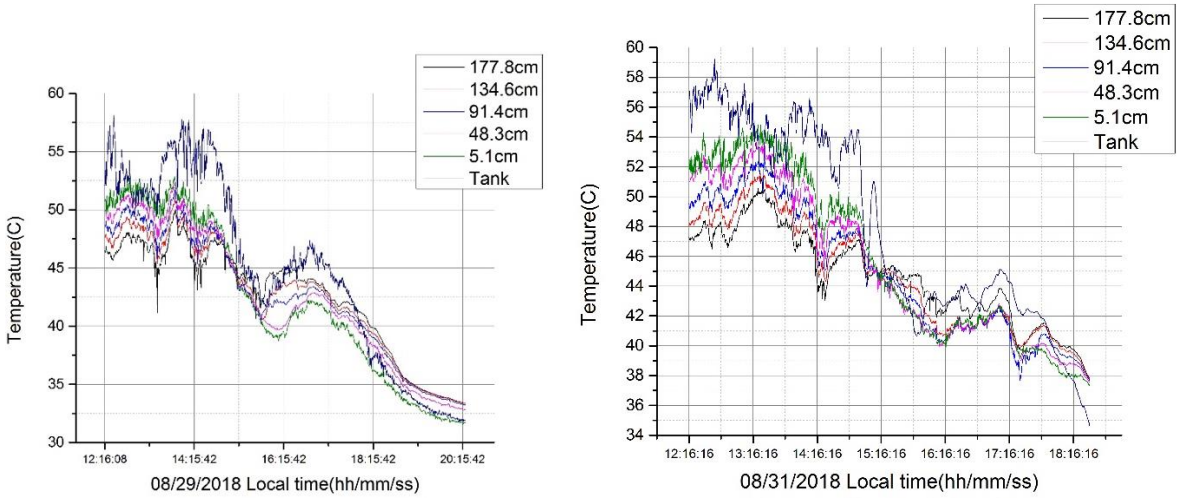

(a) top opening D=17.5mm (b) top opening D=9.5 mm

Fig. 10 Temperature of the air-water vapor mixture inside the chimney along the chimney height

Table 1: Aluminum chimney with different opening at the top of the chimney

8/29/18 (opening D=17.5mm)		8/31/18 (opening D=9.5mm)	
Time	(g water)	Time	(g water)
10:40-11:58	12	10:30-11:00	4
11:58-12:22	22	11:00-11:36	5
12:22-12:41	17	11:36-12:00	8
12:41-12:59	16	12:00-12:30	21
12:59-13:27	20	12:30-13:00	23
13:27-13:49	15	13:00-13:30	27
13:49-14:15	15	13:30-14:00	20
14:15-14:40	10	14:00-14:40	24
14:40-15:20	4	14:40-15:00	8
		15:00-15:30	5
Total	131		145

2.3.2.4 The effect of height of the chimney

The height of the chimney contributes to the water production in two aspects, the maximum driving force for the airflow that can go into the chimney by thermal syphon effect, and the maximum cooling capacity (due to heat transfer surface area) to condense the water vapor into liquid inside the chimney. The higher the chimney can be, the better the water production rate can be achieved if other conditions are the same. This has been observed from the tested data in Table 2, where the higher chimney was able to collect more water.

Table 2 The difference of water production with chimney in different heights

$H_{chimney}$=112 cm		$H_{chimney}$=182.9 cm	
Time	Collected water (g)	Time	Collected water (g)
11:30-12:00	7	10:30-11:00	4
12:00-12:30	14	11:00-11:36	5
12:30-13:00	14	11:36-12:00	8
13:00-13:30	14	12:00-12:30	21
13:30-14:00	13	12:30-13:00	23
14:00-14:30	8	13:00-13:30	27
14:30-15:00	5	13:30-14:00	20
		14:00-14:40	24
		14:40-15:00	8
		15:00-15:30	5
total water	75		145

Chapter 3. Lab test on parameters affecting the desalination performance

3.1 Lab test system layout and designs (1×1m system, 2×2m system)

3.1.1 Lab-test system layout

Based on the general ideal and old design, the new design was comprehensively updated. As the proof experiment's result showed before, simultaneous analysis of the influence factors of water generation under the variable boundary condition are infeasible, in which analysis based an in-lab experiment with constant boundary condition is required. For trying to simulate the solar radiation heat during an in-lab experiment, an additional heating pad with insulation board section is added. Therefore, the total experiment concept is organized by three parts, the heating pad section, water basin section and cooling chimney section.

Fig. 11 Design of new system

In order to take full advantage of the chimney section, the dry air needs to be sufficiently mixed with water vapor. Thus, the water basin should have sufficient area to satisfy this

purpose. Two water basins with different sizes were made for testing out the extreme cases. Each water basin is constituted by the water container, support frame and clear polycarbonate glass. The first water basin is made by a rectangular cuboid with an inner length and width of 1 m and an inner height of 0.1 m. The thickness of it is 0.003174 m (1/8 in). 10 holes with a diameter of 0.03 m each were drilled horizontally and 0.0762 m (3 in) above the bottom on each sidewalls of the water basin. For avoiding support frame, the 10 holes will be split into two groups equally, and the distance between each hole in the same group is 0.08 m. Inside the basin, a support frame is used to support both chimney and polycarbonate cover. It's organized by 4 limbs and a center hollow cylinder, the distance between the center of the cylinder and the end of the limb is 0.5m. Under each limb, there are three legs with 0.0746 m height located at 0 m, 0.1778 m and 0.3476 m from the end of limb. The center cylinder is 0.0254 m high with an inner and outer diameter equal to 0.254 m and 0.2794 m. It has 4 legs under it with 0.0762 m width and 0.0746 m height. On the top of the cylinder, a groove with 0.27305 m diameter and 0.003175 m depth is cut to fix the chimney. Detail force applied with displacement figures is shown in Appendix section B. The 4 cover pieces are made by 0.503175 m square polycarbonate sheet with a thickness of 0.0045 m and one of the corners cut off by a quarter circle with a 0.1365 m (5.375in) radius. The second water basin is an enlarged version of the first water basin. The changed parameters are shows as follows: inner length of the base of the rectangular cuboid changes to 2m; the distance between the limb and the center of the cylinder of support frame also extend to 1m; the three legs under the limb will then change their location to 0m, 0.4318m and 0.8476m, and the cover pieces are extend to 1.003175m square polycarbonate sheet. One thermocouple will be put into the water basin to test out the mean water temperature.

The new chimney is made out of 6061 Aluminum and is 3.048 m high with 0.009525 m thickness. It has an inner and outer diameter of 0.254 m and 0.27305 m. There will be 34

pairs of thermocouples applied on the chimney. Straight from the bottom, at the height 0.3048 m, 0.5588 m, 0.8128 m, 1.0668 m, 1.3208 m, 1.5748 m, 1.8288 m, 2.0828 m, 2.3368 m, 2.5908 m and 2.8448 m. There are three pairs of thermocouples applied at each height: one is located at the center, one touches the inner surface of the chimney and one touches the outer surface of the chimney. One extra thermocouple is applied at the bottom of the chimney to test out the entrance temperature. As usual, the outer surface of the chimney is polished for reflecting the solar radiation. A hollow cone holder with 0.2032 m height and an upper diameter of 0.249m is wielding at the bottom which can hold approximately 1 cubic decimeter of water and avoid obstructing the movement of the air flow. Three support legs are applied on the chimney to shear the weight of the chimney and prevent it from falling from an inclined ground and wind load. As Fig. 11 shows, three extra legs will also be applied to lock the three supporting legs, thus reinforcing the structure.

Four conic caps are designed to observe the effect of outlet size to the condensation rate. All four conic caps have the same height as 0.2286 m. The top narrowed opening of four caps has diameter of 0 m, 0.0254 m, 0.0508 m and 0.0762 m which means 0%, 10%, 20% and 30% of the chimney inner diameter.

Detailed Soildworks drawing of the above structures can be found in Appendix A.

3.1.2 Design analysis

Both the water basin and support frame are made of 5052 Aluminum, compared to 6061-T6 Aluminum, 5052 Aluminum has a lower strength which makes it easier to fabricate. It also has lower corrosion resistance than 6061-T6 Aluminum, however, it still has high corrosion resistance, which is the most important property for a container which needs to reserve warm saltine water for long periods of time.

When the load is applied to the bottom support frame, the maximum stress effect on it will be 3.413*10^5 N/m^2 for 1m size and 3.471 N/m^2 for 2m size. The stress will then cause a

maximum 2.506*10^{-4}mm and 2.552*10^$^{-3}$mm displacement of the 1m and 2m support frame which can be ignored. Thus, this data proves the structure is strong enough to support the chimney and polycarbonate glass. Detailed Soildworks simulation can be found in Appendix B.

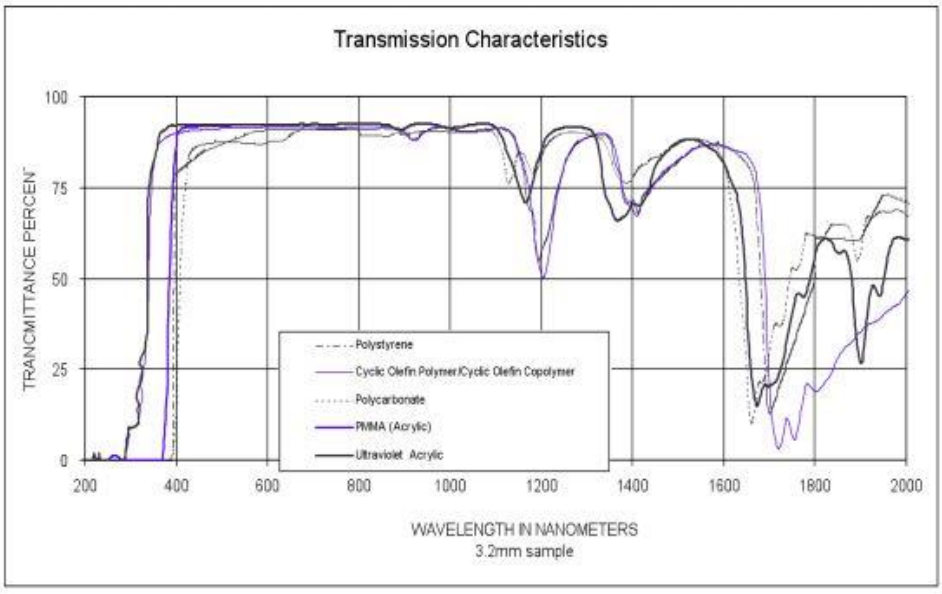

Fig. 12 [14] Transmission characteristics of optical polymers

As shown in Fig. 12 below, the radiation transmission of polycarbonate is very similar to the glass at all wavelengths, which proves both polycarbonate and glass can be chosen as the transmission cover of the basin. However, as shown above in Table.3, the advantages of polycarbonate are low thermal conductivity, high impact resistance and a cheaper price. According to these three merits, polycarbonate is able to provide a lower cost, lower maintenance cost, and better solar energy collection.

Table 3: Transmission Materials Properties

Material	**Glass**	**Polycarbonate**
Form	Solid	Solid
Light transmission	>95%	88~90%
Max service temperature	>200 ℃	120 ℃
Glass transition temperature	600 ℃	145 ℃
Thermal conductivity	1.38 W/m*K	0.173-0.210 W/m*K
Impact resistance	10J	200J
Cost (per-1m^2 piece)	$482	$109

3.2 Mass and heat transfer analysis

3.2.1 General properties of moist air

When air is mixed with water vapor, many of its properties are changed. Therefore, before the thermal analysis, it is always important for the researcher to be familiar with the properties of the moist air. Normally, a hydrometer can test out the relative humidity, dry bulb and wet bulb temperature. Dry bulb temperature the moist air temperature measured by a thermometer; wet bulb temperature represents the temperature measure by a thermometer which is warped by a wick moistened with water; relative humidity is the ratio of partial pressure of vapor and saturated vapor pressure at the same temperature. Those three properties are normally measured in an experiment for finding out the absolute humidity by using the psychometric chart shown in Fig.13.

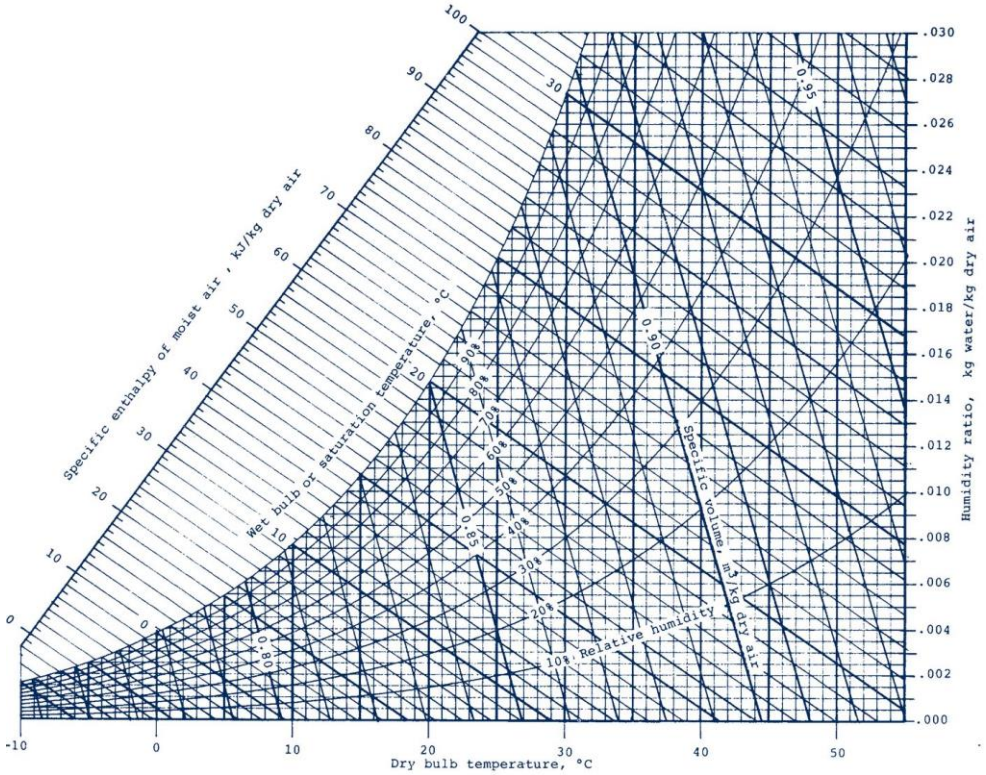

Fig.13 psychometric chart

Absolute humidity, also as known as humidity ratio, is equal to $x=\frac{m_v}{m_a}$, where m_v and m_a mean the mass of vapor and dry air. Density and heat capacity of the moist air can be calculated based on the humidity ratio. Recall that the density equation is shown in chapter 2 and the heat capacity of moist air can be calculated as:

$$c_p=\left(1.0029+5.4\cdot 10^{-5}\cdot T\right)+x\cdot\left(1.856+2\cdot 10^{-4}\cdot T\right) \tag{10}$$

The viscosity of moist air can be calculated by using equations defined by Morvay et al [15] as shown below:

$$\mu=\frac{\mu_A}{1+\phi_{AV}\cdot x_m}+\frac{\mu_V}{1+\frac{\phi_{VA}}{x_m}} \tag{11}$$

Where:

$$\phi_{AV}=\frac{\left[1+\left(\frac{\mu_A}{\mu_V}\right)^{0.5}\cdot\left(\frac{m_V}{m_A}\right)^{0.25}\right]^2}{2\sqrt{2}\cdot\left(1+\frac{m_A}{m_V}\right)^{0.5}}\qquad \phi_{VA}=\frac{\left[1+\left(\frac{\mu_V}{\mu_A}\right)^{0.5}\cdot\left(\frac{m_A}{m_V}\right)^{0.25}\right]^2}{2\sqrt{2}\cdot\left(1+\frac{m_V}{m_A}\right)^{0.5}} \tag{12}$$

$$x_m = 1.61x \tag{14}$$

$$\mu_A \cdot 10^6 = 0.40401 + 0.074582 \cdot T - 5.7171 \cdot 10^{-5} \cdot T^2 + 2.9928 \cdot 10^{-8} \cdot T^3 - 6.2524 \cdot 10^{-12} \cdot T^4 \tag{15}$$

$$\mu_v \cdot 10^6 = \frac{\sqrt{\frac{T}{647.27}}}{0.0181583 + 0.0177624 \cdot \left(\frac{647.27}{T}\right) + 0.0105287 \cdot \left(\frac{647.27}{T}\right)^2 - 0.0036744 \cdot \left(\frac{647.27}{T}\right)^3} \tag{16}$$

Here, M_A and M_V are the molar mass of dry air and vapor which are equal to 29 and 18 kg/kmol.

3.2.2 Heat and mass transfer analysis in basin

For a traditional solar distillation system, heat transfer can be separated by internal heat transfer and external heat transfer, our solar collection water basin has a similar heat transfer system. The difference in between the traditional solar distillation system and our new solar collection system is the convection heat transfer between the water surface and inner surface of the glass cover. As we introduced before, the solar distillation system is organized by a top opened insulated box with a glass cover sealed on top. As a result, the region between the water surface and inner surface of the glass cover forms a closed system, the temperature difference between water surface and inner surface of the glass cover lead to a natural convection heat transfer. As a comparison, our system has an air flow inlet and outlet which is connect to the cooling chimney section which changes the closed system into an opened system. In section 2.2, the result is proved as the pressure of the water basin inlet is higher than the pressure at the bottom of the chimney (also consider as the outlet of the water basin), this results in the air flowing across the section as a Poiseuille flow. As a result, the convection heat transfer of the region is enhanced, which will also enhance the water evaporation heat transfer and reduce the water condense rate at the inner surface of the glass cover. The reduction of the water condense rate can maintain the clearness of the glass then maintain the transmission of the solar irradiation, otherwise, the water condensed on the inner surface of the glass will create another water membrane which will increase the reflection of solar irradiation, resulting in the reduction of solar energy collection. Here, a general heat transfer simulation of the solar distillation system and our new concept will show below, for easy understanding, the general heat transfer of the whole system can be classified into internal and external heat transfer.

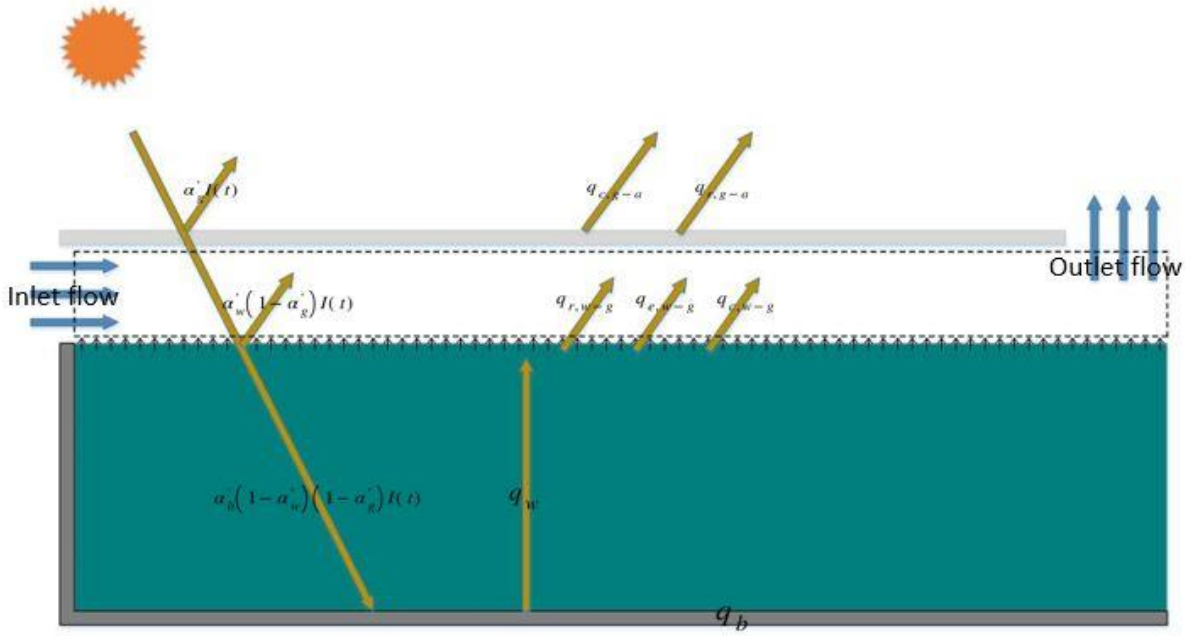

Fig.14 Energy diagram of water basin

3.2.2.1 Internal heat transfer

Internal heat transfer of the water basin section can be represented by two parts, heat transfer inside the water and heat transfer from the water surface to the inner surface of the glass. The water heat transfer will mainly consist of convection and evaporation. Heat transfer in between the water surface and inner surface of the glass is organized by convection, evaporation, and radiation. Convection and evaporation heat transfer for both parts happen simultaneously, thermal radiation heat transfer between the water surface and inner glass surface occurs independent of the former two types of heat transfer.

Radiation heat transfer

Compared to the length of the channel created by the covered glass and water surface, the width in between them is negligible, thus, the view factor between the water surface and inner surface of the glass cover is considered as unity. Therefore, the rate of radiation heat transfer can be written as:

$$q_r = h_{r-wg}\left(T_w - T_{ig}\right) \tag{17}$$

Where $h_{r\text{-}wg}$ means the thermal radiation coefficient in between the water surface and inner glass surface and can be defined as:

$$h_{r-wg} = \varepsilon_t \sigma \left(T_w + T_{ig}\right)\left(T_w{}^2 + T_{ig}{}^2\right) \tag{18}$$

Which here ε_t means the effective emissivity and will be equal to:

$$\varepsilon_t = \left(\varepsilon_w{}^{-1} + \varepsilon_{ig}{}^{-1} - 1\right)^{-1} \tag{19}$$

Convection heat transfer

After many years developing, a general equation can be used for most solar stills or fully closed distillation system defined by Zheng et al [16] as:

$$h_{c,w-g} = \frac{0.2\left(Ra'\right)^{0.26} K_v}{X^v} \tag{20}$$

Where

$$Ra' = \frac{X_v^3 \rho_v g \beta}{\mu_v \alpha_v} \Delta T'' \tag{21}$$

And

$$\Delta T'' = \left[\left(T_w - T_{ig}\right) + \frac{P_w - P_{ig}}{\dfrac{M_a P_t}{Ma - Mv} - P_w}\left(T_w\right)\right] \tag{22}$$

Here, M_a and M_v mean the molar mass of dry air and vapor. μ, α, β, and X mean the dynamic viscosity, thermal diffusivity, thermal expansion, and characteristic length.

The side section of this new design water basin can be considered as a parallel plat chancel. Dry air flowing in can be considered as Poiseuille flow, therefore, the convection heat transfer coefficient based on the temperature profile is equal to $h_{c,w-g} = \frac{NuD_H}{k}$, where $D_h = 4H$ and Nu =8.2353. In reality, the convection heat transfer in here is more complicated than either a natural convection or a forced convection. As a result, the velocity profile of the air flow will

not change as usual since the density of air changes. During the evaporation of water, the rising of the vapor will also create a vertical flow that will effect both momentum and energy equations. Hence, there will be a new Nusselt number instead of 8.2353, this part will be analyzed in future work.

Evaporation

For a fully closed solar still, as Dunkle's developed [17]

$$q_{e,w-g} = h_{e,w-g}\left(T_w - T_{ig}\right) \tag{23}$$

Where $h_{e,w-g}$ is the evaporation coefficient and will be equal to

$$h_{e,w-g} = 16.273\times 10^{-3}\times h_{c,w-g}\left(\frac{P_w - P_{ig}}{T_w - T_{ig}}\right) \tag{24}$$

For this new concept, since it is not a fully closed system anymore, it is important to know what the parameters that influence the water evaporation are. Generally, the evaporation of a free water surface will be affected by the solar radiation and water surface air flow velocity. Researchers used aerodynamic methods and energy methods to derive the equation as:

Aerodynamic method:

$$E_a = \frac{0.622k^2\rho_a u_2}{P\rho_w\left[\ln\left(\frac{Z_2}{Z_0}\right)\right]}\left(P_{vs} - P_{va}\right) \tag{25}$$

Energy method:

$$E_r = \frac{I\cdot t}{\gamma} \tag{26}$$

Where, P is the total pressure and P_{vs}, P_{va} are the partial pressure of vapor at the water surface and ambient air based on the temperature profile, k is relative humidity. γ is the latent heat water requires for evaporation.

After combining the two methods above to get a more accurate evaporation rate, the equation can be defined as:

$$E = \frac{\Delta}{\Delta + \gamma_c} E_r + \frac{\gamma_c}{\Delta + \gamma_c} E_a \tag{27}$$

Where

$$\gamma_c = \frac{C_p D_c P}{0.622 \gamma K \alpha} \qquad \text{And} \qquad \Delta = \frac{4098 P_{vs}}{(237.3 + T)^2}. \tag{28-29}$$

Recall from the introduction, the air flow crosses in between 2 parallel plates than flow across a plate like a ground or water surface. Hence, the velocity profile under this condition is different from it under a free water surface. As a result, these above equations will be re derived with the new velocity profile from same porocedure. Before the future analysis of the velocity profile, the evaporation rate will be written as:

$$E = \frac{(25 + 19V) A(x_s - x)}{3600} \tag{30}$$

Where V is the velocity and x_s is the humidity ratio of saturate moist air.

3.2.2.2 External heat transfer

External heat transfer also consists of two parts, heat loss from the outer surface of the glass cover and heat loss from the side and bottom wall. For the first part, the heat loss is caused by convection created by ambient air flow and thermal radiation from the glass surface to the sky. The heat loss for the second part is due to conduction heat transfer of the basin and the insulate material.

The external radiation heat transfer can be defined as:

$$q_{r,g-a} = h_{r,g-a}(T_{og} - T_a) \tag{31}$$

At here, $h_{r,g-a}$ means the radiation coefficient of glass and equal to

$$h_{r,g-a} = \varepsilon_g \sigma \left[\frac{T_{go}^4 - T_{sky}^4}{T_{go} - T_a} \right] \tag{32}$$

Where $T_{sky} = T_a + 6$ [18].

The external convection heat transfer can be defined as:

$$q_{c,g-a} = h_{c,g-a}\left(T_{og} - T_a\right) \tag{33}$$

At here, $h_{r,g-a}$ means the convection coefficient of glass, as Tiwari[18] defined, the relationship between wind speed and convection coefficient of glass is equal to:

$$h_{c,g-a} = 2.8 + \left(3.0 + v_a\right) \tag{34}$$

As section 3.1.1 shows, the outer surface of the water basin will be wrapped by an insulation layer, similar to the internal radiation heat transfer, side wall conduction heat transfer can be ignored since it is small compared to the bottom area of the water basin. Therefore, the heat transfer equation can be defined as:

$$q_b = \frac{K_b}{X_b}\left(T_{ib} - T_{ob}\right) + \frac{K_{ins}}{X_{ins}}\left(T_{ob} - T_g\right) \tag{35}$$

Where K_b, X_b, K_{ins} and X_{ins} mean the conductivity and thickness of the water basin bottom and the insulate material. T_{ib}, T_{ob} and T_g mean the temperature at water basin, inner surface, outer surface and round.

3.2.2.3 Water basin energy balance simulation

As a summary of the above analysis, with solar energy applied, energy balanced equations will be set up in this section. Recall from the introduction, a solar distillation system is mainly consisted of solar energy and heat. Solar energy is the input energy source. The solar energy is trapped and transferred into heat by a solar collector. Once the heat is absorbed by water, the total water desalination system will begin operating.

The whole simulation will be separated into four parts which are at specific temperature points, they are shown as follows:

The first energy balanced equation is used to simulate the heat transfer at the inner surface of the glass cover

$$\alpha_g^{'} I(t) + q_{r,w-g} + q_{c,w-g} + q_{e,w-g} = \frac{K_g}{X_g}\left(T_{ig} - T_{og}\right) \tag{36}$$

Where α_g' means the absorbance of the glass cover and I(t) means the intensity of solar radiation over the glass cover.

The second energy balanced equation is used to simulate the heat transfer at the outer surface of the glass cover

$$\frac{K_g}{X_g}\left(T_{ig} - T_{og}\right) = q_{r,g-a} + q_{c,g-a} \tag{37}$$

The third energy balanced equation is used to simulate the heat transfer at the water surface

$$\alpha_w^{'}\left(1 - \alpha_g^{'}\right) I(t) + q_w = \dot{m} c_p \frac{dT}{dt} + q_{r,w-g} + q_{c,w-g} + q_{e,w-g} \tag{38}$$

Where α_w' means the absorbance of water

The fourth energy balanced equation is used to simulate the heat transfer at the water basin bottom

$$\alpha_b^{'}\left(1 - \alpha_b^{'}\right)\left(1 - \alpha_w^{'}\right) I(t) = q_w + q_b \tag{39}$$

Where α_b' means the absorbance of water basin bottom.

3.2.4 Energy balance analysis in condensation tower

The flow structure inside the chimney is similar to the solar power plant which we can consider as an in-pipe flow with forced and natural convection happening simultaneously. In this paper, the natural convection part inside the chimney will be ignored since it is small compared to the forced convection. Therefore, the heat transfer from the center of the chimney to the surrounding area will be shown as Fig.15

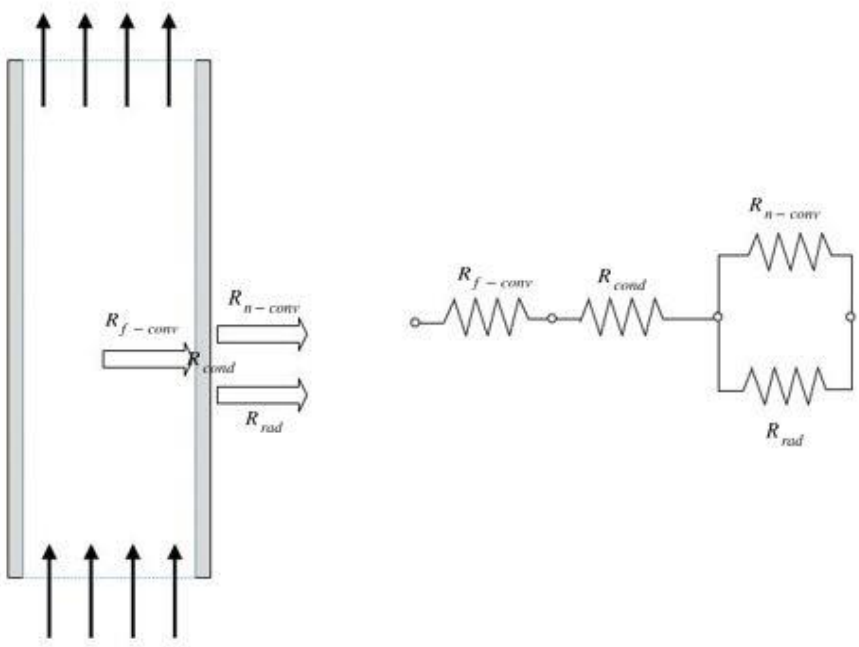

(a) Sideview of tower/chimney (b) Thermal circuit of chimney heat transfer at same level

Fig. 15 Energy diagram of the chimney

Thus, the thermal resistances in Fig. 15 fore-and-aft each represents, forced convection resistance, thermal conductive resistance, natural convection resistance, and thermal radiation resistance.

Forced convection resistance can be written as

$$R_{f-conv} = \frac{1}{h_i A_i} \tag{40}$$

Here, A_i means the inner surface area and hi means the forced convection coefficient which can be defined as

$$h_i = \frac{Nuk}{D} = \frac{0.023 Re^{0.8} Pr^{0.3} k}{D} \tag{41}$$

Here, Nu means the Nusselt number, D is the inner diameter of the chimney, the Nusselt number can also be written as the equation shows. Here, Re is the Reynold's number which is defined as $Re = \frac{\rho u D}{\mu}$ and Pr is the Prandtl's number which is equal to $Pr = \frac{c_p \mu}{k}$. k, ρ, μ and c_p means

the thermal conductivity of the chimney wall, density of the moist air, dynamic viscosity of moist air and heat capacity of the moist air.

Thermal conductive resistance can be written as:

$$R_{cond} = \frac{1}{2\pi Lk} \ln\left(\frac{r_o}{r_i}\right) \tag{42}$$

Where r_i and r_o means the inner and out radius, L means the length of the chimney and k means the thermal conductivity of the chimney wall.

Natural convection resistance can be written as:

$$R_{n-conv} = \frac{1}{h_o A_o} \tag{43}$$

Here, A_o means the inner surface area and ho means the natural convection coefficient which can be defined as

$$h_o = \frac{Nuk}{D} \tag{44}$$

Where Nusselt number will be redefined as

$$Nu = \begin{cases} 0.59Ra^{\frac{1}{4}} & 10^4 < Ra < 10^9 \\ 0.1Ra^{\frac{1}{3}} & 10^9 < Ra < 10^{13} \end{cases} \tag{45}$$

Here, Ra means the Rayleigh number and will be equal to $Ra = Gr \cdot Pr$, which Gr is the Grashof number and will be equal to $Gr = \frac{\rho^2 g\beta\left(T_o - T_\infty\right)D^3}{\mu^2}$. Here, T_∞ means the ambient temperature and β means the thermal expansion of ambient air and will be assumed as $\beta = T_f^{-1} = \left(\frac{T_o + T_\infty}{2}\right)^{-1}$.

Thermal radiation resistance will be written as:

$$R_{rad} = \frac{1}{h_r A_o} \tag{46}$$

Here, h_r means the thermal radiation coefficient and will be defined as

$$h_r = \varepsilon_r \sigma_r \left(T_o + T_\infty \right) \left(T_o^2 + T_\infty^2 \right) \tag{47}$$

Where ε_r is the emissivity of the chimney outside wall and σ_r is the Stefan-Boltzmann constant which is equal to 5.67*10^-8 W/m^2-K^4.

Therefore, the general energy balanced equation will be formed as:

$$h_i \left(T_m - T_w \right) = \frac{2\pi Lk}{\ln\left(\frac{r_o}{r_i} \right)} \left(T_i - T_o \right) \tag{48}$$

$$\frac{2\pi Lk}{\ln\left(\frac{r_o}{r_i} \right)} \left(T_i - T_o \right) = h_o \left(T_o - T_\infty \right) + h_r \left(T_o - T_\infty \right) \tag{49}$$

From heat exchange simulation, after combined all thermal resistance, the general thermal coefficient can be written as:

$$\overline{U} = \frac{1}{A_i R_{tot}} = \frac{1}{\frac{1}{h_i} + \frac{r_i}{k} \ln\left(\frac{r_o}{r_i} \right) + \frac{r_i}{r_o} \frac{1}{h_o + h_r}} \tag{50}$$

Therefore, by simplifying the energy balance equations, the heat loss from the pipe can be defined as:

$$q = \overline{U} A_i \Delta T_{lm} \tag{51}$$

Here, ΔT_{lm} is the temperature difference between inner and outer surface, which is equal to

$$\Delta T_{lm} = \frac{\Delta T_o - \Delta T_i}{\ln\left(\frac{\Delta T_o}{\Delta T_i} \right)} \tag{52}$$

Temperature of the inner surface will be represented by T_i. The Chimney is used to cool the moist air flowing through it, based on energy conservation, the heat loss by the flow from inlet to outlet should match the heat released by the chimney, therefore, q should also be equal to:

$$q = \dot{m}_{air} Cp_{air} (T_{in} - T_{out}) + \dot{m}_{w-in} Cp_w (T_{in} - T_{out}) + \dot{m}_{w-cond} \cdot r \quad (53)$$

$\dot{m}_{air}$ is obtained based on chimney flow calculation is the bottom temperature . This can also decide the volume flow rate $\dot{V}_{in}$ of air going to the chamber.

$$\dot{m}_{w-cond} = \dot{m}_{w-in} - \dot{m}_{w-out} \quad (54)$$

Where $\dot{m}_{w-in} = \frac{p_{sat} \dot{V}_{in}}{R_w T_{in}}$ and $\dot{m}_{w-out} = \frac{p_{sat-out} \dot{V}_{in}}{R_w T_{out}}$ assuming that the volume flow rate $\dot{V}_{in}$ is about the same as that of air flow.

Heat transfer equations (from bulk flow to air) should get the q from above. The condensation heat transfer coefficient of steam is very large and the thermal resistance is negligible. If T_{in} is known, T_{out} needs to be assumed and then calculated for comparison and iteration. Because T_{out} is not known, it will be assumed, then calculate the heat q using the enthalpy equation. Also, the heat transfer can calculate a q. If the two q are not the same, T_{out} will be assumed again and until the q are the same.

3.3 Experimental analysis

3.3.1 Experimental set up

The in-lab experimental test will be run under a constant room temperature of 23.6 ~ 23.8°C. Before starting the test, water will be filled into the water basin until the water level reaches 5cm. During the pretest, the changes of the evaporation rate can be ignored when the water level difference is under 0.5cm, which means measuring the water level difference under constant time will reflect the evaporation rate. At this stage, a concept structure organized by a fully opened and fully closed chimney with 1m water basin will be tested out under constant temperature. The detailed plans are:

1.1 When the concept with 1 m^2 basin is under a fully opened chimney situation, with a constant power output, which is 1kw/s, find out the steady state temperature.

1.2 At constant temperatures of 30°C, 35°C, 40°C and 44°C, measure out the evaporation and condensation rate of the 1 meter square basin concept.

2.1 When the concept with 4-meter square basin is under a fully open chimney situation, with a constant power output which is 4kw/s, find out the steady state temperature.

2.2 At constant temperatures as 30°C, 35°C, 40°C and 44°C, measure out the evaporation and condensation rate of the 4-meter square basin concept.

During the experiment, the temperature profile of water, inner/outer surface of chimney and humid air inside the chimney will again be monitored using NI data acquisition system operated using Labview. The relative humidity and dry bulb temperature will be able to be measured out by a hydrometer and the velocity profile of inlet and outlet will be measured by a hand held flow meter with uncertainty under 0.015m/s. The outlet will connect to a container, water inside the container will be filled into a glass graduate after each 10 to 20 minutes to measure out the amount of water generation.

3.3.2 Experimental result

3.3.2.1 Evaporation rate at different temperature with fully opened outlet

1 m^2 water basin

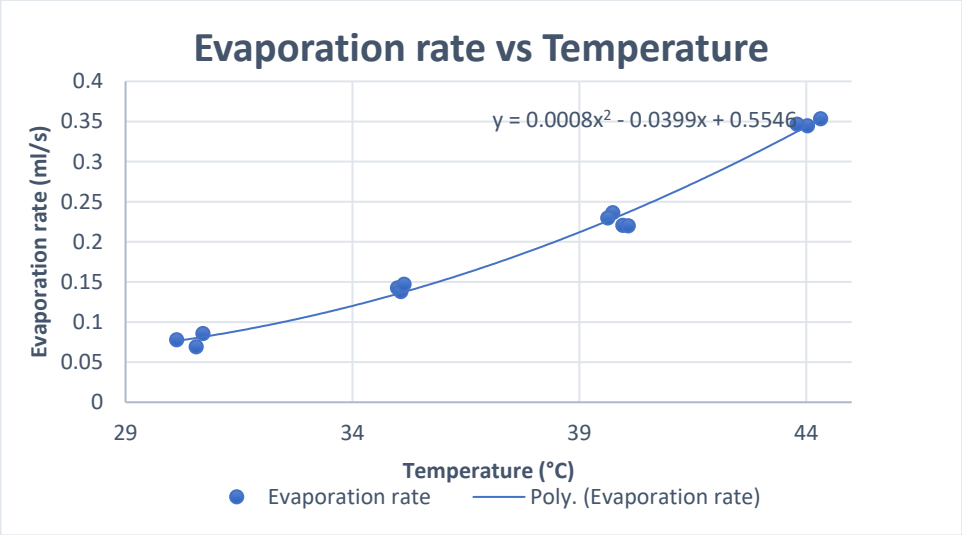

Fig.16 Evaporation rate at different temperature (1 m^2)

The evaporation rate at different temperatures is shown in Fig. 16. The evaporation rate increases as a second order polynomial function while temperature increases. Under the chimney outlet fully opened situation, a 1 kW power output heat pad functioning under full power can only heat up and remain the water temperature as 44.8°C, which means at steady state, 1kw/m^2 power can provide 0.353ml/s evaporation rate and keep the water at 44.8°C simultaneously. During the experiment, the highest water-temperature can increase to 45 °C with a depth of water inside the basin increase from 5cm to 5.4cm, in the other hand, the full power functioning heat pad can only keep the water temperature at 43.6°C while the depth of water drops to 3cm. This result is matching the previous studies of the solar still property, which is as thin the water depth as large the evaporation rate. This is caused by the volume of the gas region, when there is less water, the partial volume of gas inside basin increase, then enhances either the natural convection or forced convection, therefore the evaporation rate is increased.

4 m^2 water basin

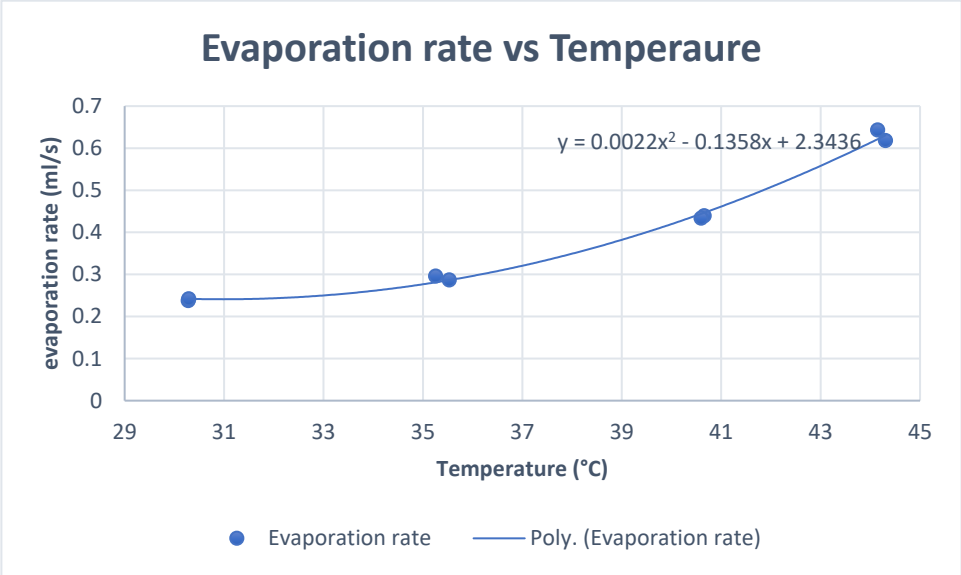

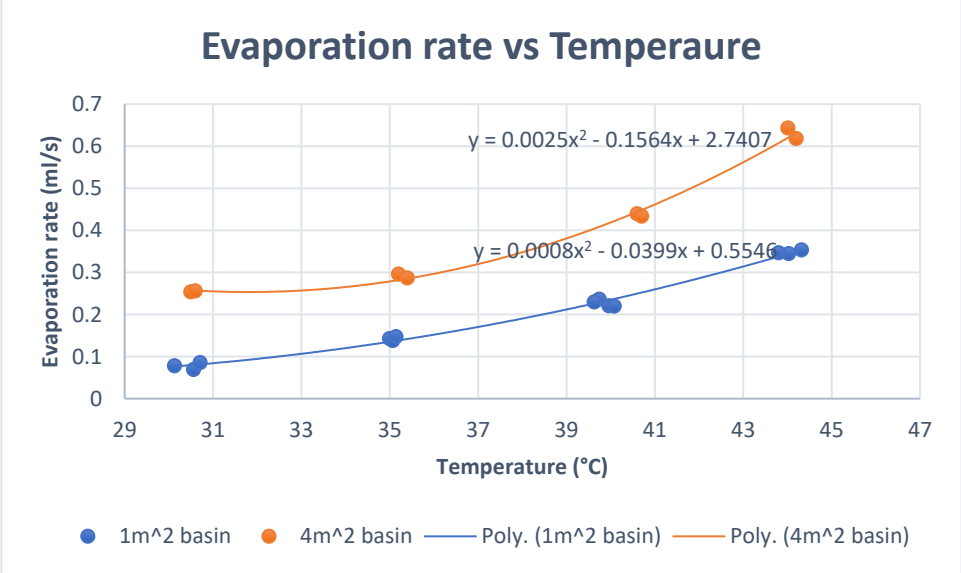

Fig.17 Evaporation rate at different temperature (4 m^2)

Compared to the 1-meter square basin, the total evaporation rate of the 4 m^2 basin increases faster. However, as Fig.18 shows below, if the evaporation rate of the 4 m^2 water basin converts to pre meter square, both magnitude and increasing rate of it under each temperature are reduced.

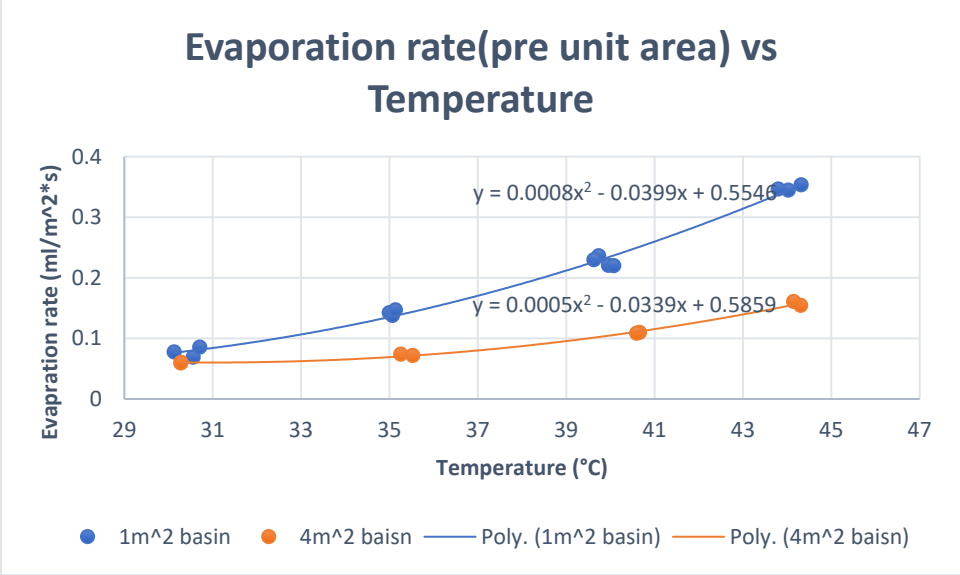

Fig. 18 Evaporation rate pre meter square at different temperature

Based on the experiments, the relative humidity of 4m^2 water basin reaches 100% before the air fluid flows into the chimney, meanwhile, the relative humidity reaches 100% at the center of the 1m^2 water basin. The result leads to the relative humidity difference inside the chimney. That will cause the air to be unable to carry more water vapor flow across the near center region, therefore reducing the evaporation rate.

3.3.2.2 Air flow rate at different temperature with fully opened outlet

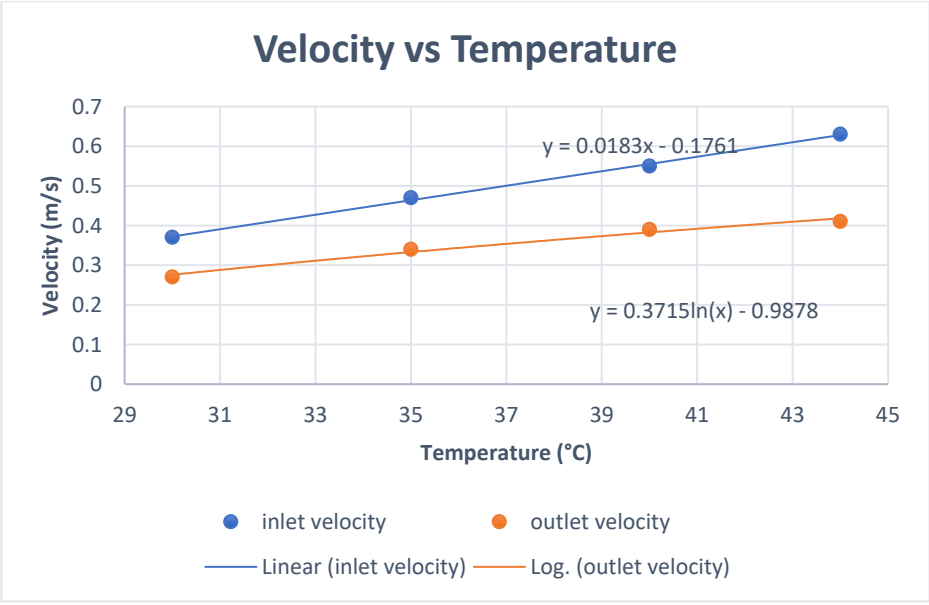

Fig. 19 Velocity of inlet and outlet at different temperature (1 m^2)

As shown in Fig. 19, the velocity difference between the inlet region and outlet region is increasing with the increase of water temperature. Recall from section 3.2, the evaporation rate is increasing with the increase of the water temperature. Therefore, absolute humidity inside the water basin is increasing with the increase of the water temperature. As a result, the density of air inside the water basin is decreasing with the increase of the water temperature. From ideal gas law, air pressure is proportional to the air density, thus air pressure inside the basin is decreasing with the increase of the water temperature. Since the ambient air pressure is constant, combine to the result, the pressure difference between ambient air and moist air in the basin is increasing with the increase of the water temperature. Higher pressure difference then leads to high velocity. The convection is then enhanced when temperature rises and provides a higher mass transfer rate. The increase of humidity ratio will further decrease the density ratio, and then create an even higher-pressure difference. These two processes simultaneously happening will make the velocity of the inlet become faster and faster. The decrease of the increasing rate of outlet velocity is caused by the increase of temperature difference between the in-pipe air and ambient air. The increase of temperature difference will reduce the maximum relative humidity. Thus, the water that will be transferred back to the liquid phase can stay in vapor phase. Then increase the water condensation rate. According to the equation $\dot{m}_{condense} = \dot{m}_{in} - \dot{m}_{out}$, if the increasing rate of condensation rate and inlet mass flow rate are close to each other, then the outlet mass flow rate should approach a constant, therefore the velocity of outlet will also approach a constant.

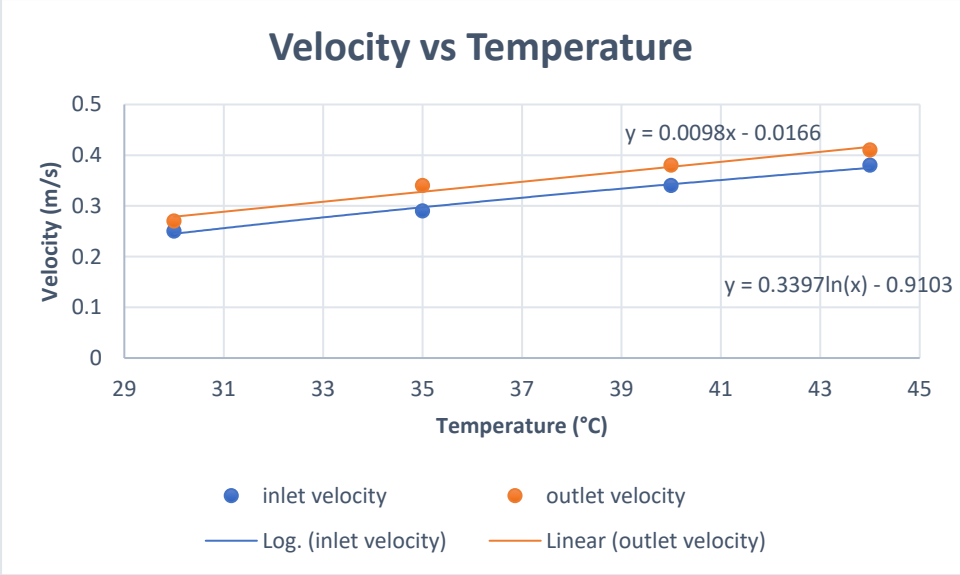

Fig. 20 Velocity of inlet and outlet at different temperature (4 m^2)

Compared to the 1m^2 water basin, the 4m^2 basin has a lower inlet velocity and same outlet velocity profile (Fig. 20), which proves why the evaporation rate pre meter reduced. As section 3.2.2.1 mentioned, the evaporation heat transfer and convection heat transfer happened simultaneously. When the moist air is saturated, the air convection heat transfer is mainly affected by the natural convection, which means the velocity normal to the ground shows more influence compared to the inlet velocity parallel to the water surface. That is why the inlet velocity decrease, herein the evaporation rate per meter square decrease.

3.3.2.3 Heat loss through the chimney

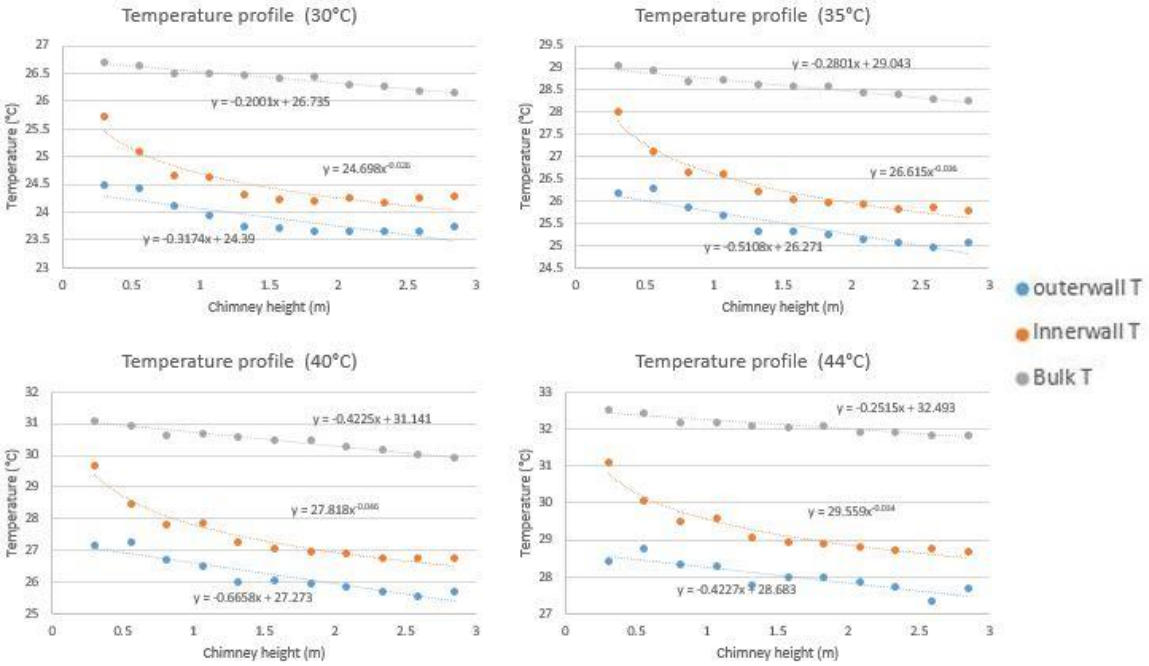

Fig.21 Temperature profiles at constant water temperature (1 m^2 basin)

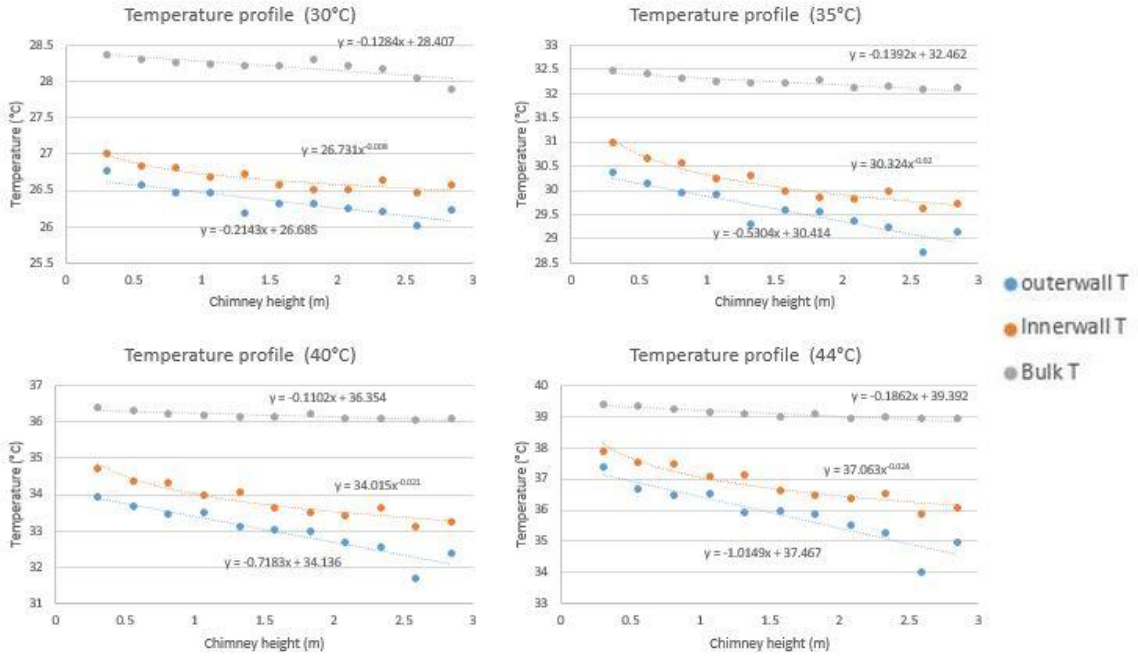

Fig.22 Temperature profiles at constant water temperature (4 m^2 basin)

The difference between the basin sizes will also affect the generation of water. As the temperature profile shown in Fig.21 and Fig.22, there is a big temperature difference between the bulk flow and chimney inner surface, which is caused by the heat loss from the chimney. This heat loss can lead to the condensation of gasified water. However, when the relative humidity is lower than 100%, the condensed water dew will be reheated by the high temperature air flow and then be gasified into steam again. When the volume of water drop is large enough, the surface tension will be broken, which makes the re-gasification of water dew difficult. The phenomenon is corresponding to the data collected from 1 m^2 basin, because the relative humidity at the outlet of the chimney is under the condition of 77%, 86%, 96% and 99.9% at 30°C, 35°C, 40°C and 44°C, respectively. Thus, no water was collected at the temperature of 30°C, 35°C and 40°C, while 43 ml of water was collected at 40 °C in 10 h. Different to the 1 m^2 basin, the 4 m^2 basin could guarantee the saturated moist air flow at the inlet of the chimney, which can lead to the relative humidity at outlet of chimney reaches 99.9% at all the tested temperatures during the experiment. Therefore, the generation rates of water are 0.374 ml/min, 1.311 ml/min, 6.054 ml/min and x.xx ml/min at 30 °C, 35 °C, 40 °C and 44 °C, respectively.

4. Conclusion and Future work

The thesis investigated the in-lab performance of a new designed water desalination tower. According to the results, the size of the water basin was found to be one of the most important factors that affect the generation of water. The 4 m^2 water basin provides an enough space for the intensive mixture of the air and vapor. However, when the relative humidity reaches 100%, the gasified water starts to be condensed on the surface of the glass and drops back into the water basin. The phenomenon will lead to the reduction of air flow velocity, and further reduce the evaporation rate per m^2. Both of the reduction of the air flow velocity and the evaporation rate will waste the solar energy. Meanwhile, the small water basin with the size of 1 m^2 can provide a maximum inlet velocity of air, which will lead to a maximum evaporation rate per m^2. However, its small size will cause the inadequate mixture of vapor and air, hence the condensation rate of water inside the chimney will drop significantly.

According to the experimental data, a new water basin with a different size will be designed in the future. The relative humidity of the moist air in the new designed basin will reach 100% before the moist air flows into the chimney. The new basin should also match with the requirement of avoiding the waste of solar energy caused by an extra area of the basin. Besides, 10%, 20%, 30% and fully closed situation of this design will also be tested in the future, for better comparison between the present data and the upcoming data. The numerical analysis will be the most important research topic of this project for a better understanding of inner flow structure including the effect of condensed water on the energy (heat transfer) inside the chimney. An initial result from Fluent (a software of CFD simulation) with dry-air flow inside different sizes of this design is posted in Appendix B.

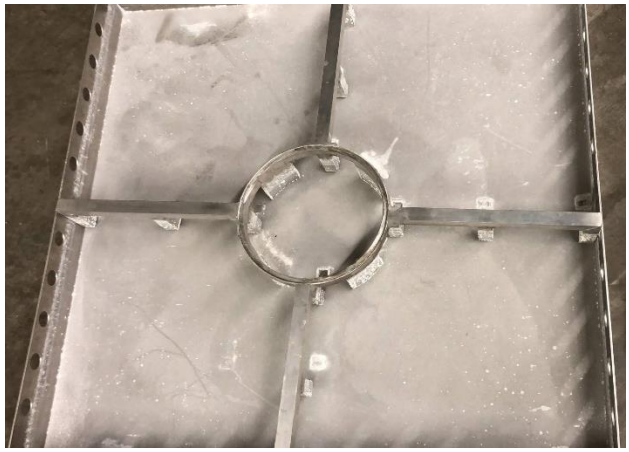

Fig. 23 Basin with remainder salt.

It is also important to design an additional system combined with the basin that can remove salt from the basin to avoid the effect to water evaporation and the corrosion of the basin.

APPENDIX

Appendix A- Concept detail Solidworks drawing

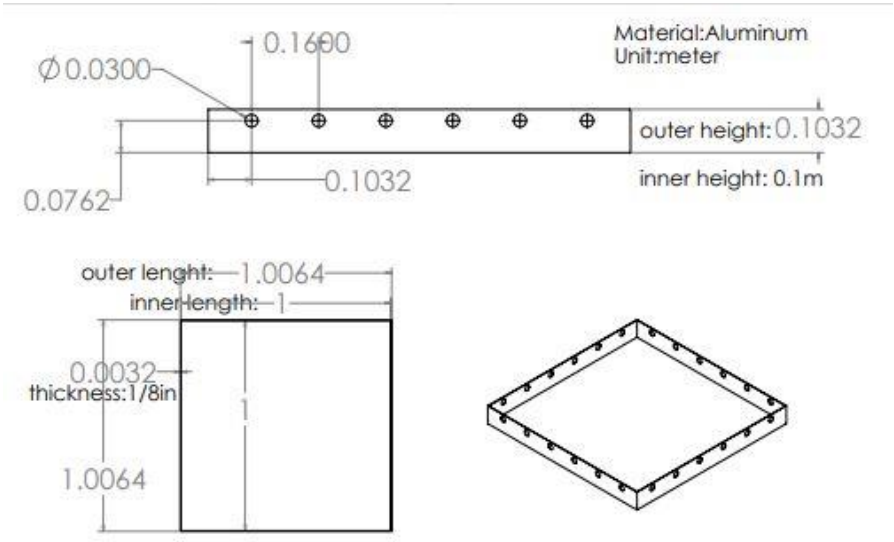

Fig A1. Detail drawing of the 1m water basin

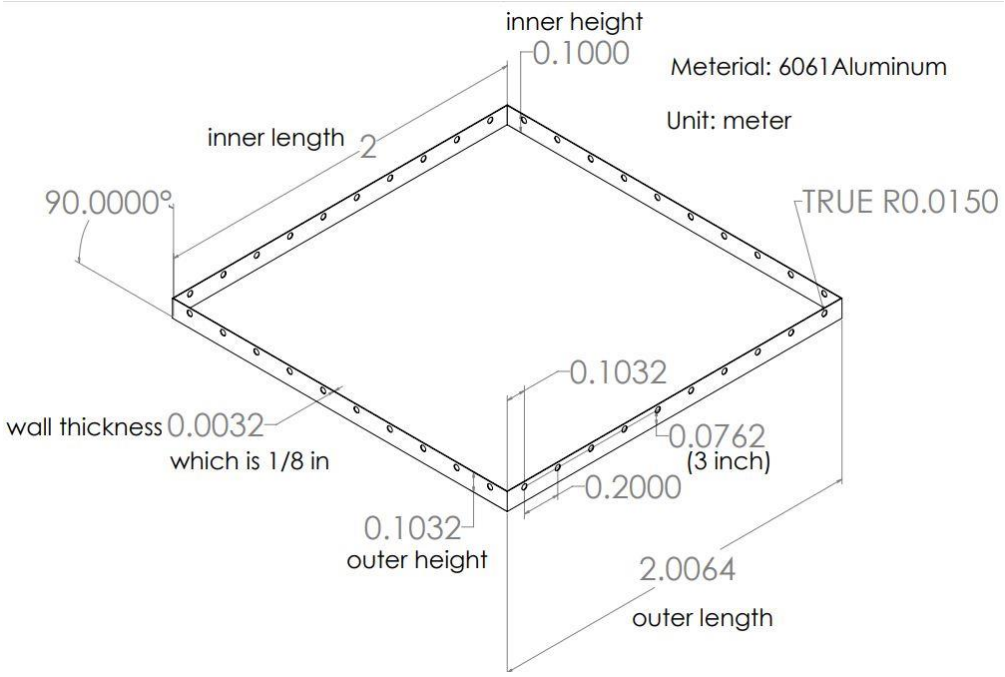

Fig A2. Detail drawing of the 2m water basin

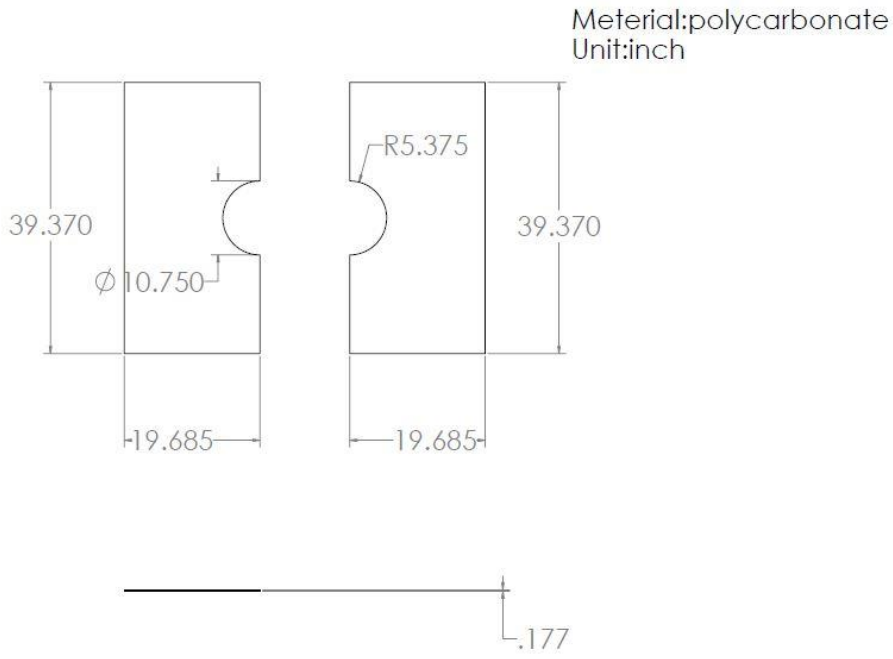

Fig A3 Detail drawing of the 1m basin polycarbonate cover

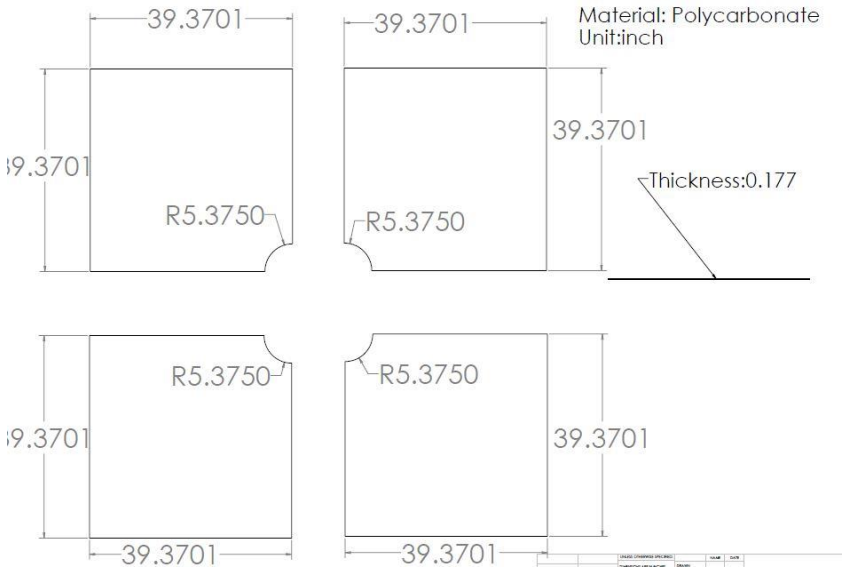

Fig A4 Detail drawing of the 2m basin polycarbonate cover

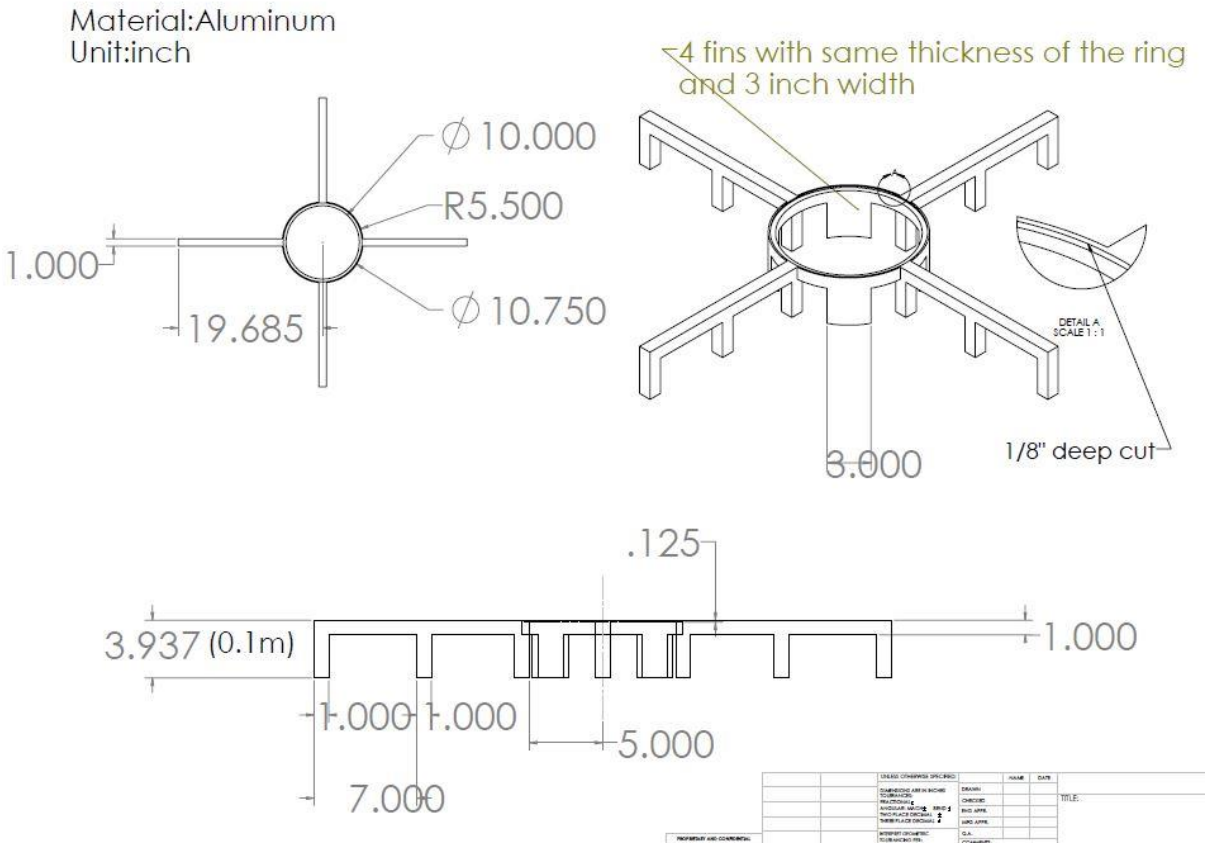

Fig A5 Detail drawing of the 1m support frame

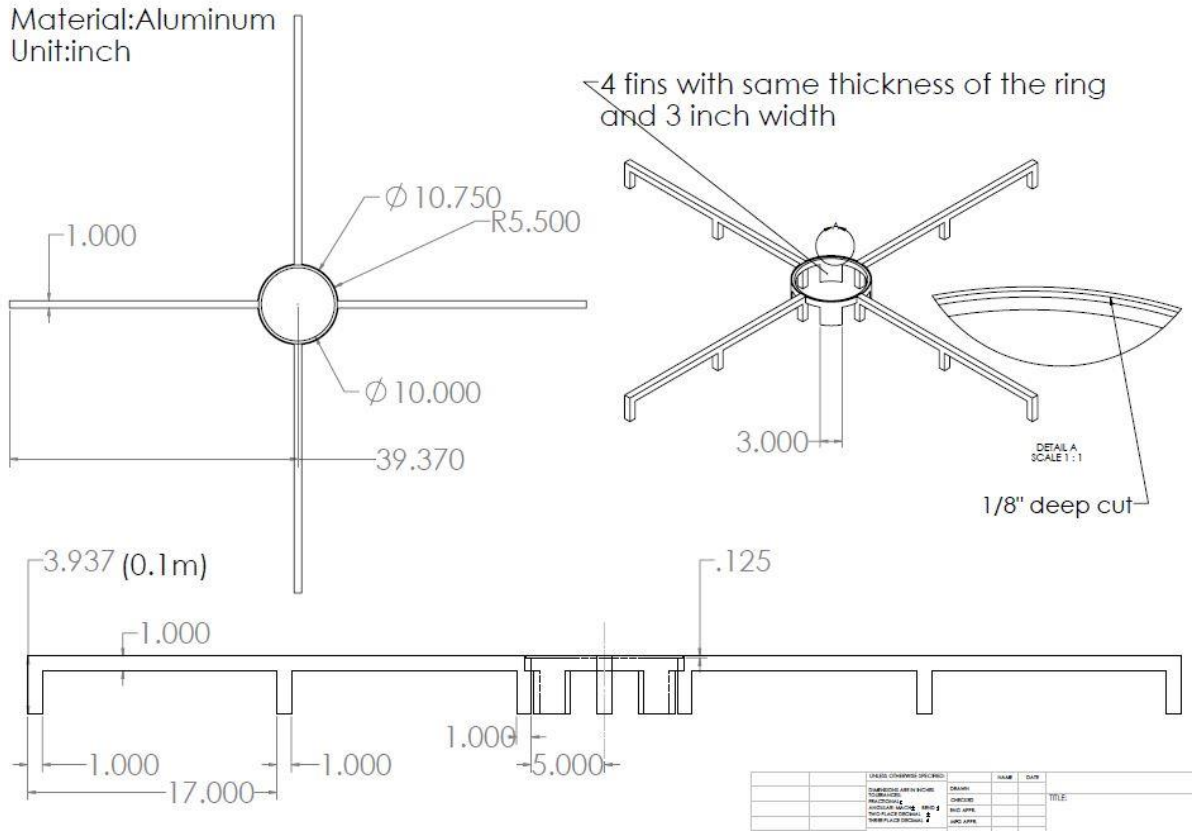

Fig A6 Detail drawing of the 2m support frame

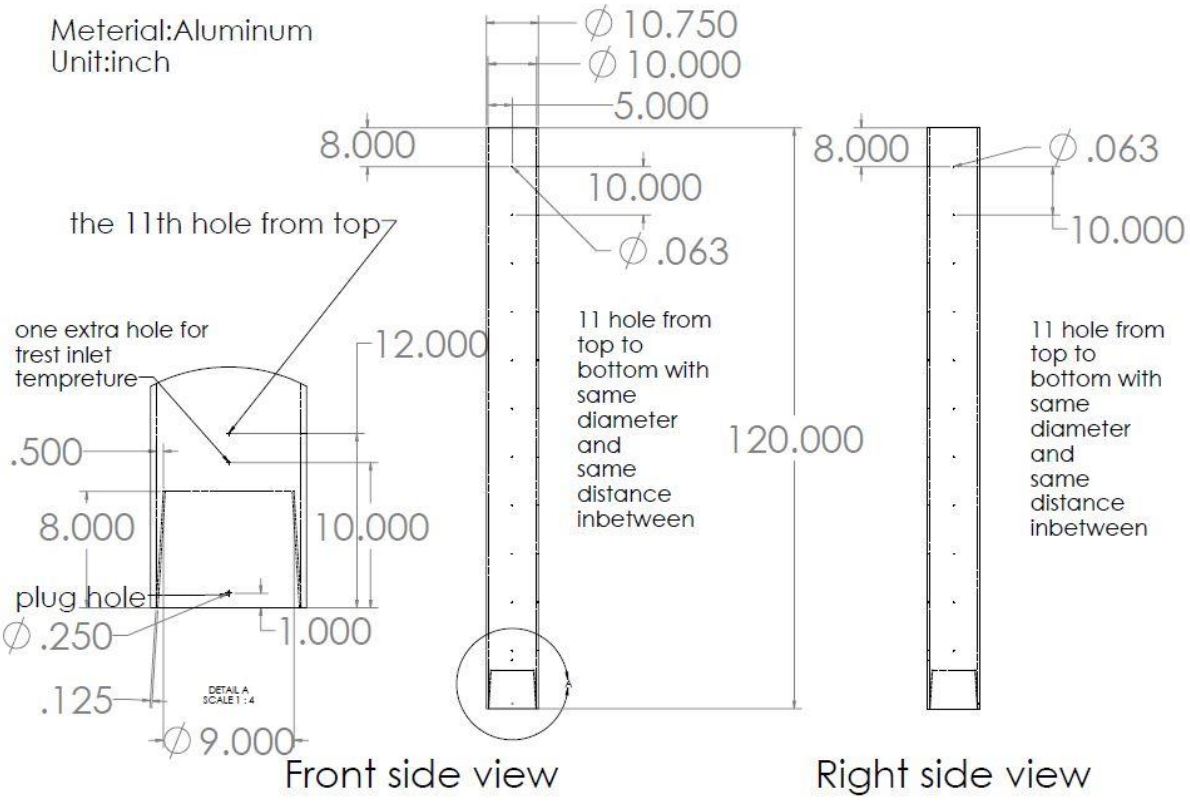

Fig A7 Detail drawing of the chimney

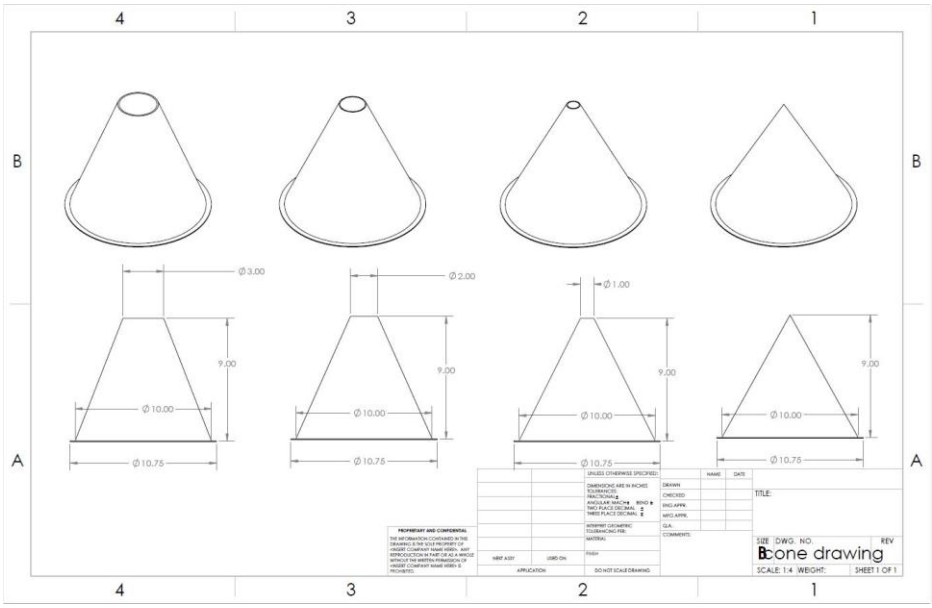

Fig A8 Detail drawing of the conic cap

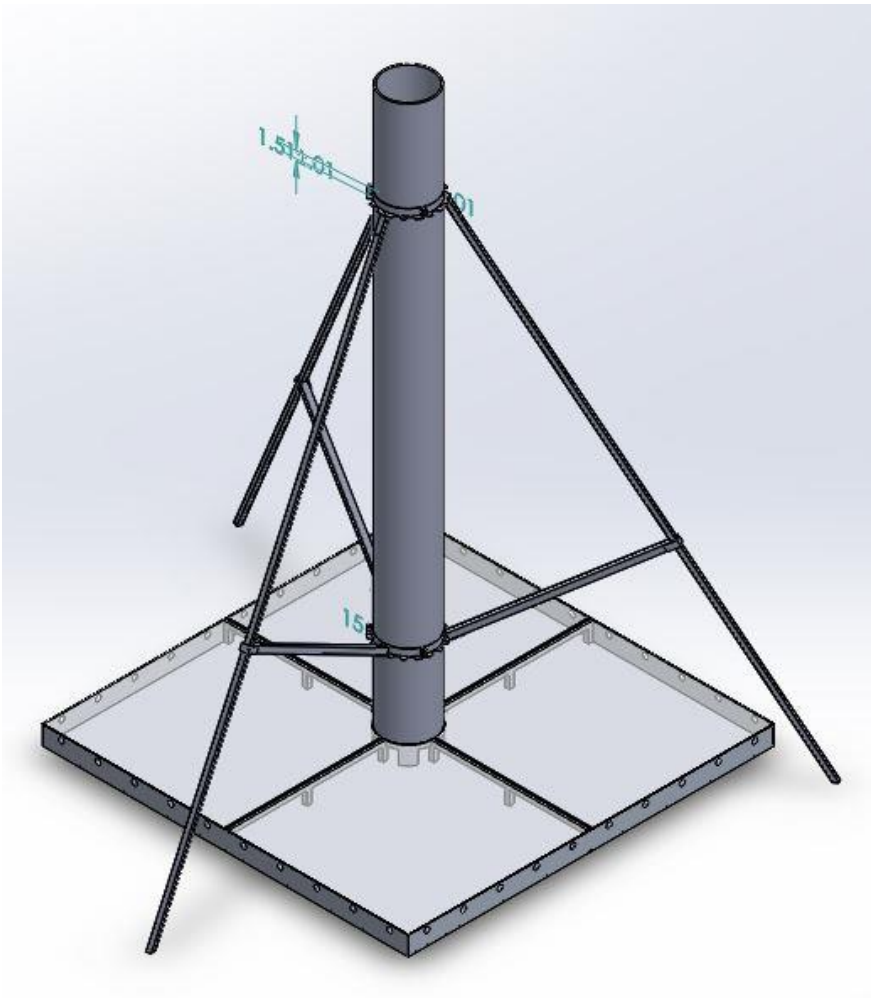

Fig A9 3D view of the project with the support legs.

Appendix B- Software simulation

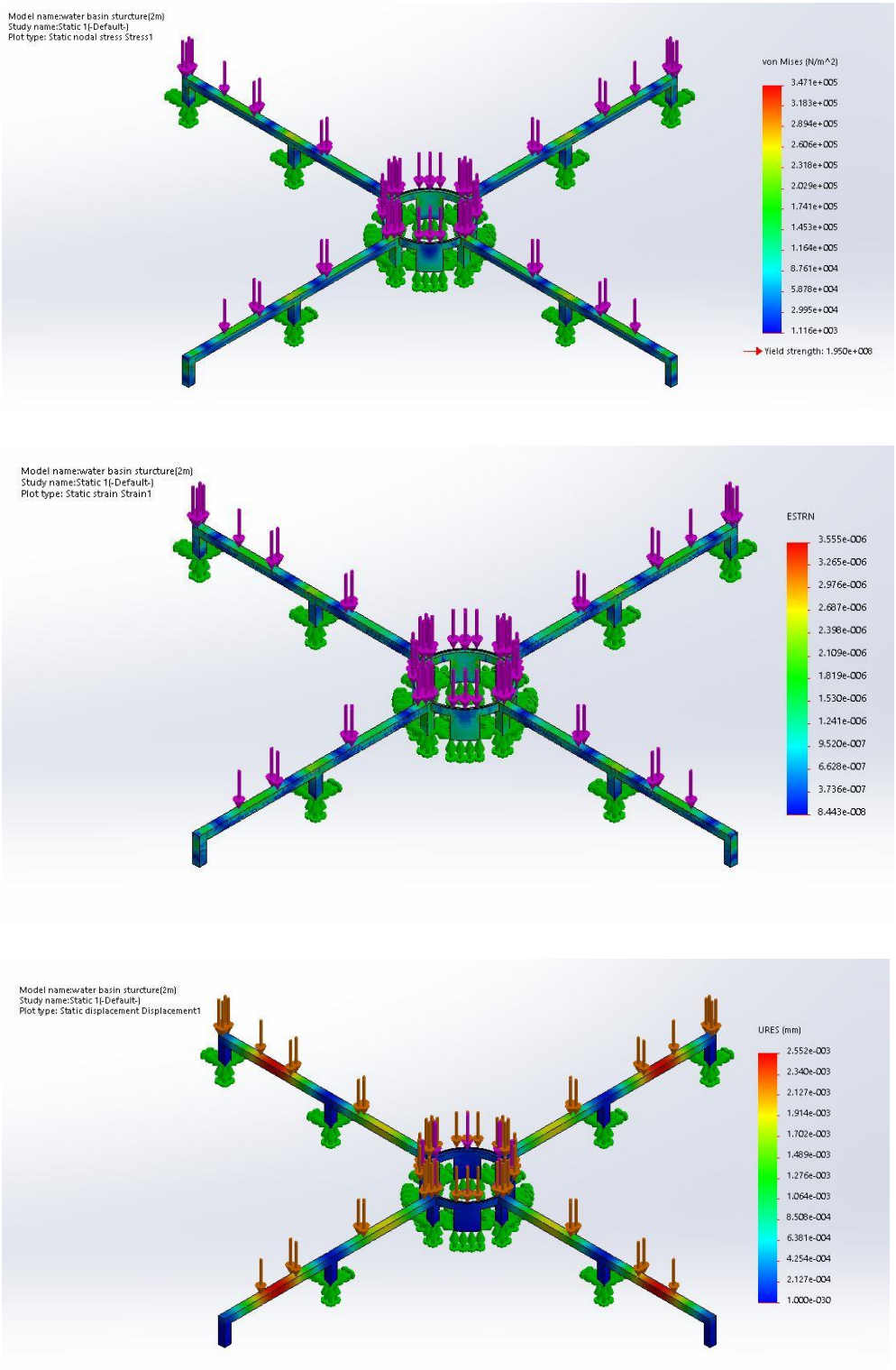

Fig B1 1m^2 water basin support structure analysis

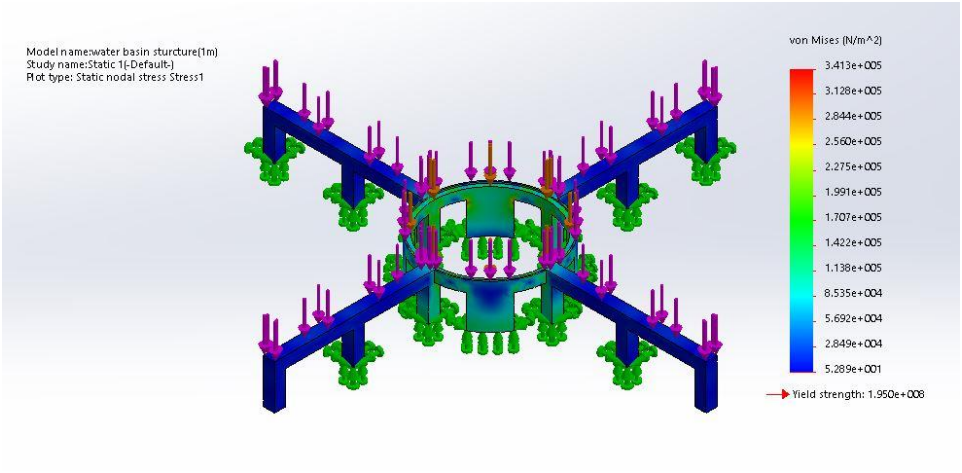

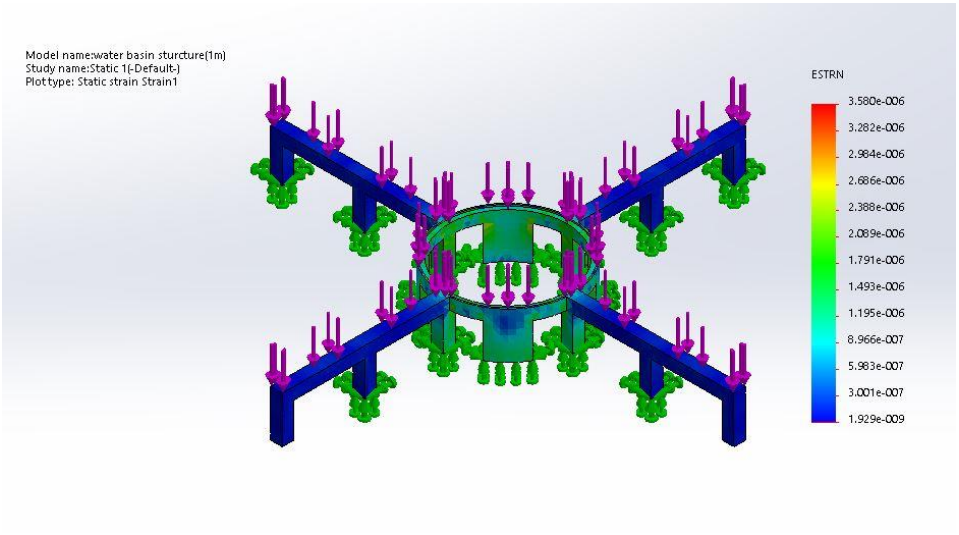

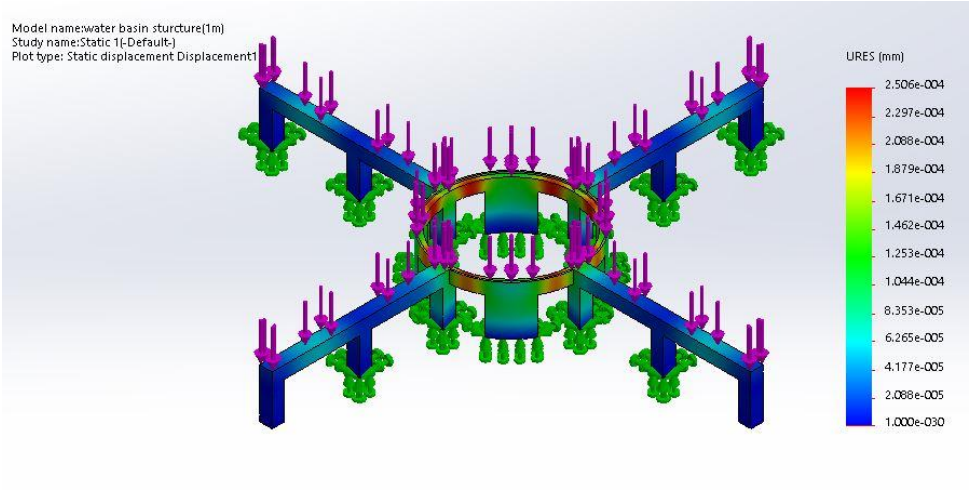

Fig B2 4m^2 water basin support structure analysis

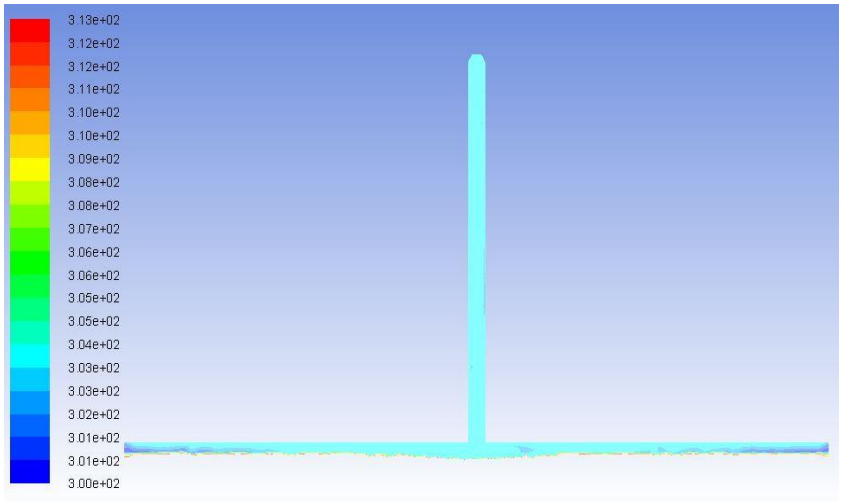

Temperature

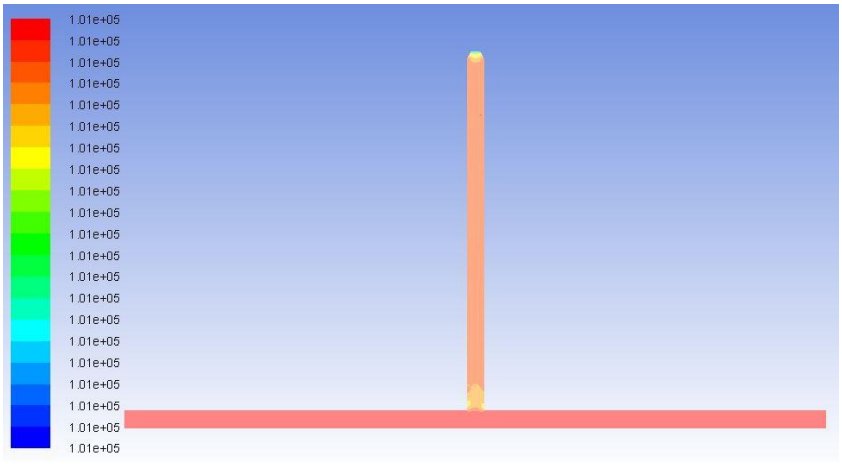

Pressure

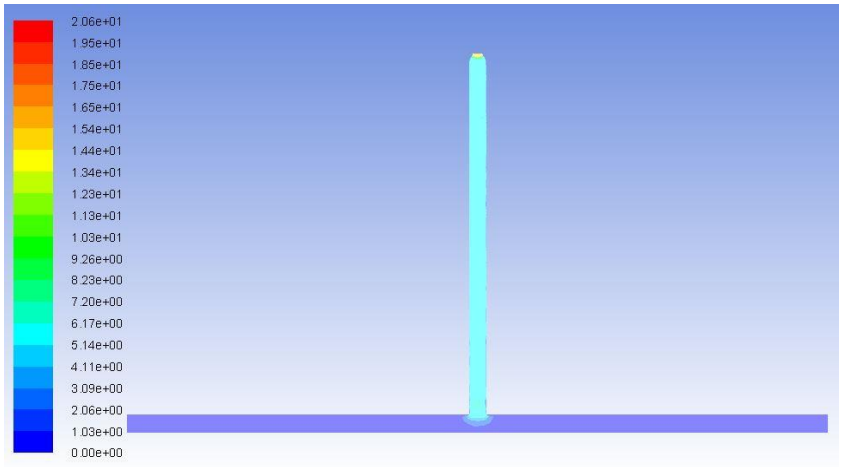

Velocity

Fig B3 Ansys dry natural convection Size 5

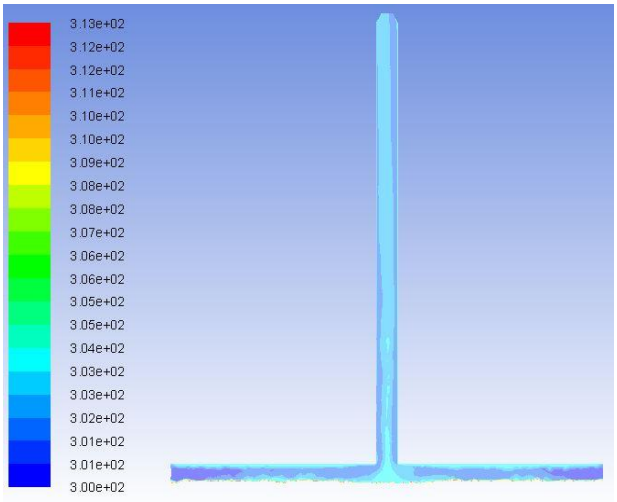

Temperature

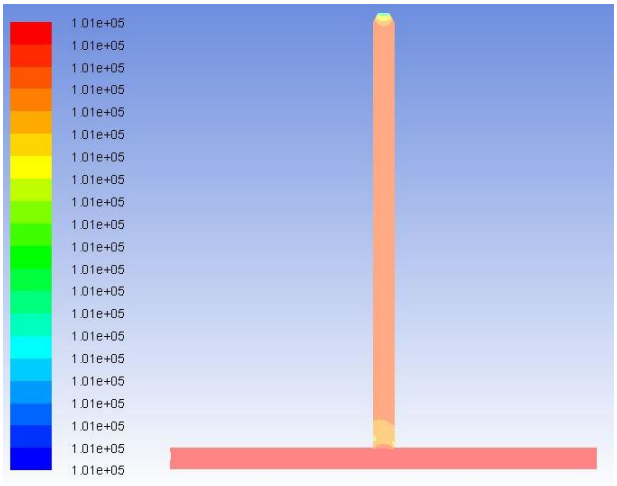

Pressure

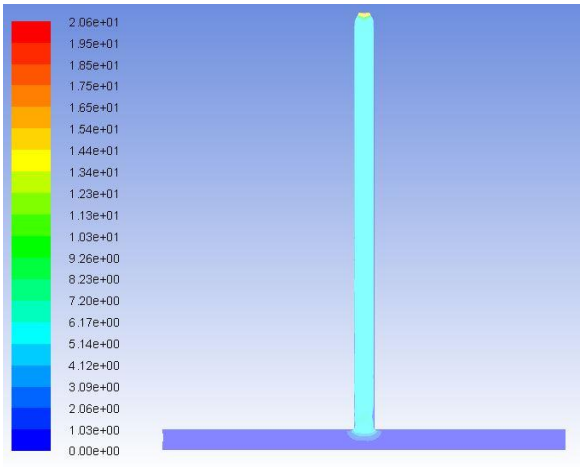

Velocity

Fig B4 Ansys dry natural convection Size 4

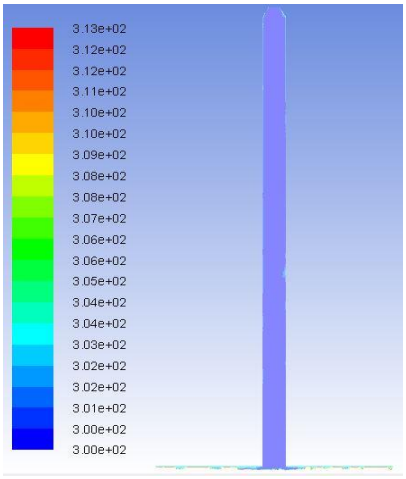

Temperature

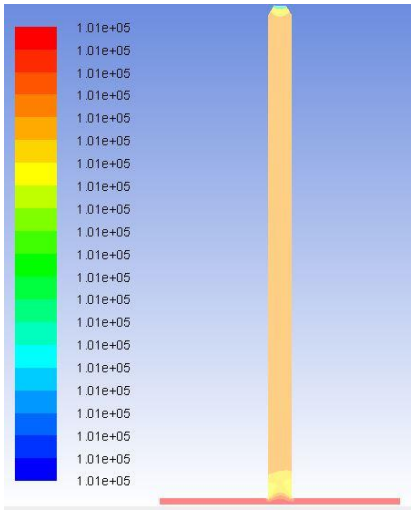

Pressure

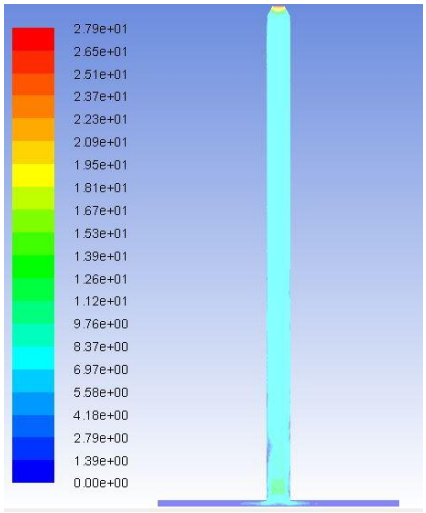

Velocity

Fig B5 Ansys dry natural convection Size 3

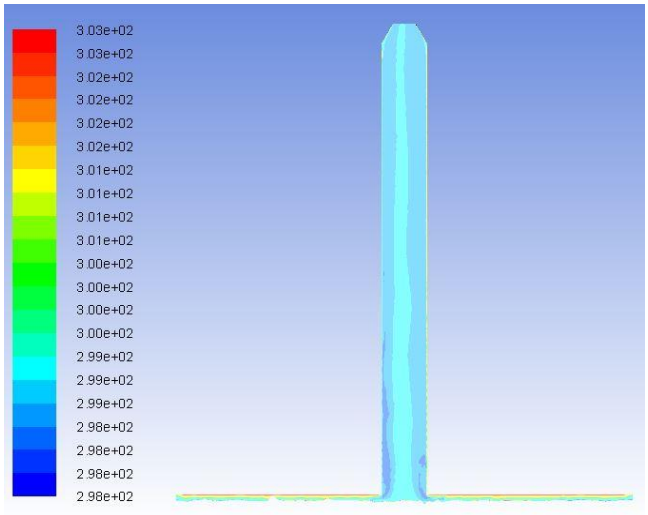

Temperature

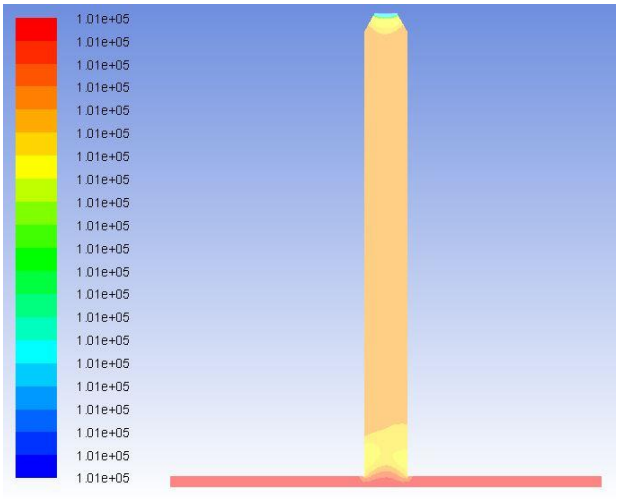

Pressure

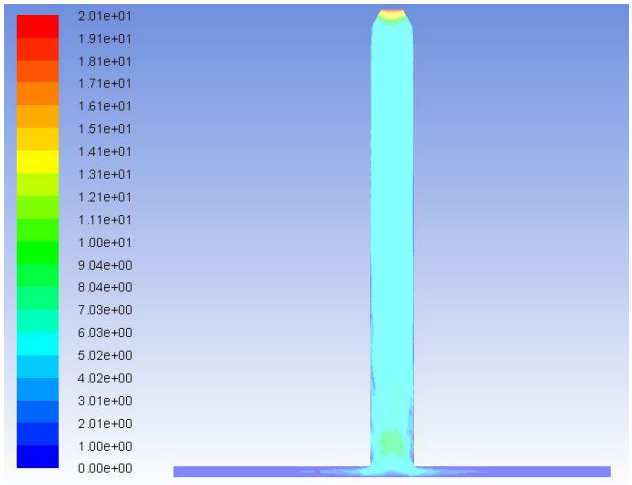

Velocity

Fig B6 Ansys dry natural convection Size 2

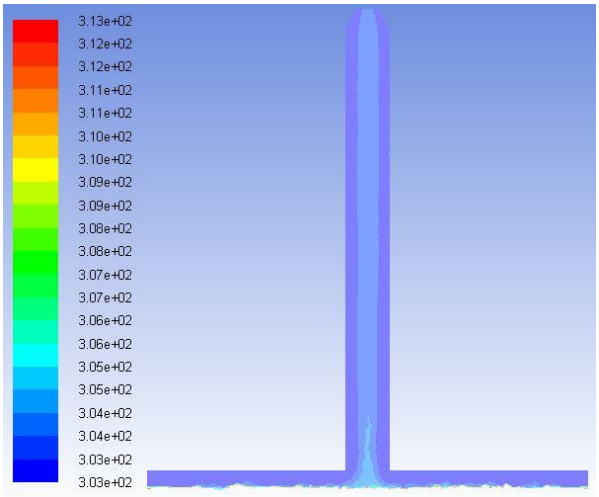

Temperature

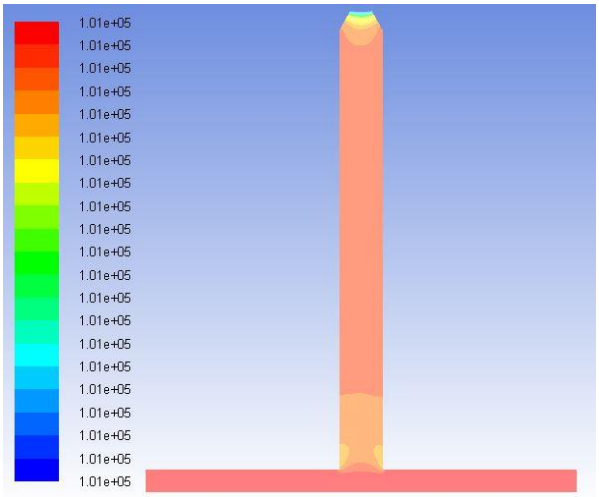

Pressure

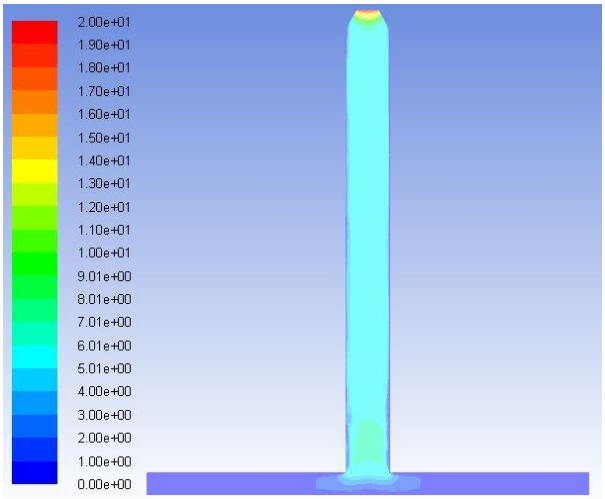

Velocity

Fig B7 Ansys dry natural convection Size 1

Table B. ANSYS Simulation

	Size1				
No. of iterations	10000	20000	50000	80000	100000
Inlet velocity(m/s)	0.237742	0.237704	0.237834	0.238169	0.237817
Outlet velocity(m/s)	19.74964	19.73268	19.73907	19.77629	19.75164
Inlet velocity(m^3/s)	14.93017	14.92784	14.936	14.95704	14.93493
Outlet velocity(m^3/s)	15.50347	15.49015	15.49517	15.52439	15.50504
Dimensions					
Tank	radius:	10 m	height:	1 m	
Chimney	radius:	1 m	height:	20 m	
Cone	radius:	1 m/0.5m	height:	0.57 m	
Boundary Conditions					
Bottom Temperature(K)	353				
Wall temperature(K)	303				
Transglass temperature(K)	303				
Inlet pressure(Pa)	101325				
Outlet pressure(Pa)	101065.8				
	Size2				
No. of iterations	10000	20000	50000	80000	100000
Inlet velocity(m/s)	0.476699	0.476008	0.476565	0.477648	0.476916
Outlet velocity(m/s)	19.73994	19.75084	19.75068	19.79268	19.74617
Inlet velocity(m^3/s)	14.96836	14.94664	14.96414	14.99813	14.97515
Outlet velocity(m^3/s)	15.49585	15.50441	15.50428	15.53725	15.50074
Dimensions					
Tank	radius:	10 m	height:	0.5 m	
Chimney	radius:	1 m	height:	20 m	
Cone	radius:	1 m/0.5m	height:	0.57 m	
Boundary Conditions					
Bottom Temperature(K)	353				
Wall temperature(K)	303				
Transglass temperature(K)	303				
Inlet pressure(Pa)	101325				
Outlet pressure(Pa)	101071.8				
	Size3				
No. of iterations	10000	20000	50000	80000	100000
Inlet velocity(m/s)	0.648413	0.663132	0.662818	0.664864	0.663086
Outlet velocity(m/s)	28.1891	27.51891	27.52619	27.57972	27.52939
Inlet velocity(m^3/s)	20.36017	20.82234	20.81249	20.87674	20.8209
Outlet velocity(m^3/s)	22.12844	21.60234	21.60806	21.65008	21.61057
Dimensions					
Tank	radius:	10 m	height:	0.5 m	
Chimney	radius:	1 m	height:	40 m	
Cone	radius:	1 m/0.5m	height:	0.57 m	
Boundary Conditions					

Bottom Temperature(K)	353				
Wall temperature(K)	303				
Transglass temperature(K)	303				
Inlet pressure(Pa)	101325				
Outlet pressure(Pa)	100825.4				
	Size4				
No. of iterations	10000	20000	50000	80000	100000
Inlet velocity(m/s)	0.250905	0.112574	0.108662	0.108806	0.108515
Outlet velocity(m/s)	12.242	20.28254	20.29022	20.28994	20.26474
Inlet velocity(m^3/s)	15.75682	7.06966	6.82398	6.833004	6.814736
Outlet velocity(m^3/s)	2.402493	3.980448	3.981956	3.981901	3.976955
Dimensions					
Tank	radius:	10 m	height:	1 m	
Chimney	radius:	0.5 m	height:	20 m	
Cone	radius:	0.5/0.25m	height:	0.144 m	
Boundary Conditions					
Bottom Temperature(K)	353				
Wall temperature(K)	303				
Transglass temperature(K)	303				
Inlet pressure(Pa)	101325				
Outlet pressure(Pa)	101070.9				
	Size5				
No. of iterations	10000	20000	50000	80000	100000
Inlet velocity(m/s)	0.124381	0.121006	0.125488	0.124181	0.157374
Outlet velocity(m/s)	20.68921	20.25865	20.26869	20.26377	20.25381
Inlet velocity(m^3/s)					
Outlet velocity(m^3/s)					
Dimensions					
Tank	radius:	20 m	height:	1 m	
Chimney	radius:	0.5 m	height:	20 m	
Cone	radius:	0.5/0.25m	height:	0.144m	
Boundary Conditions					
Bottom Temperature(K)	353				
Wall temperature(K)	303				
Transglass temperature(K)	303				
Inlet pressure(Pa)	101325				
Outlet pressure(Pa)	101070.9				

Appendix C- Solar energy collected by the basin

```
r3=50;
r4=10;
r14=50;
L=6;
q1=0.9*1353;
T2=80;
T3=80;
T4=80;
T2l=T2^4;
T3l=T3^4;
T4l=T4^4;
F11=0;
F33=0;
F44=0;
F41=0;
F14=0;
A2=2*pi*r3*L
A3=pi*r3^2
A4=pi*r4^2;
A1=A3-A4;
S31=1+(1+(r14/L)^2)/(r3/L)^2;
S34=1+(1+(r4/L)^2)/(r3/L)^2;
F314=(1/2)*(S31-sqrt(S31^2-4*(r14/r3)^2));
F34=(1/2)*(S34-sqrt(S34^2-4*(r4/r3)^2));
F31=F314-F34;
F13=A3*F31/A1;
F43=A3*F34/A4;
F32=1-F31-F33-F34;
F12=1-F11-F13-F14;
F42=1-F41-F43-F44;
F23=A3*F32/A2;
F21=A1*F12/A2;
F24=A4*F42/A2;
F22=1-F21-F23-F24;
A=[F11 F12 F13 F14
   F21 F22 F23 F24
   F31 F32 F33 F34
   F41 F42 F43 F44]
x=6/50;
n=4
F23check=0.5*(x*sqrt(4+x^2)-x^2);
B = zeros(n,n);
for rowb = 1:n
    for columnb = 1:n
        if rowb == columnb
            del = 1;
        else
            del = 0;
        end
        if columnb == 1
            ep = 0.9;
        elseif columnb == 2
            ep = 0.023;
        else
            ep = 1;
        end
        B(rowb,columnb) = (del/ep - A(rowb,columnb)*(1-ep)/ep);
    end
end
```

```
Bmatrix = B
C = zeros(n,n);
for rowc = 1:n
    for columnc = 1:n
        if rowc == columnc
            del = 1;
        else
            del = 0;
        end
        C(rowc,columnc) = 5.67*10^(-8)*(del-A(rowc,columnc));
    end
end
Cmatrix = C
unKnown=zeros(n,n);
for rowu = 1:n
    for columnu = 1:n
        if columnu ==1
            unKnown(rowu,columnu)= C(rowu,columnu);
        else
            unKnown(rowu,columnu)= B(rowu,columnu);
        end
    end
end
unKnownmatrix = unKnown
Known=zeros(n,n);
for rowu = 1:n
    for columnu = 1:n
        if columnu ==1
            Known(rowu,columnu)= B(rowu,columnu);
        else
            Known(rowu,columnu)= C(rowu,columnu);
        end
    end
end
Knownmatrix = Known
Constant=[q1; T2l; T3l; T4l];
Knownplus=Knownmatrix*Constant;
Result=unKnownmatrix\Knownplus
```

Reference:

[1] Elimelech, M. and W. A. Phillip (2011). "The Future of Seawater Desalination: Energy, Technology, and the Environment." Science 333(6043): 712-717.

[2].Seawater desalination using renewable energy sources. Author links open overlay panelSoteris A.Kalogirou

[3] Li, C. N., Y. Goswami, et al. (2013). "Solar assisted sea water desalination: A review." Renewable & Sustainable Energy Reviews 19: 136-163.

[4] J.H. Reif, W. Alhalabi, Solar-thermal powered desalination: Its significant challenges and potential, Renewable and Sustainable Energy Reviews, 48 (2015) 152-165.

[5] H. Sharon, K.S. Reddy, A review of solar energy driven desalination technologies, Renewable and Sustainable Energy Reviews, 41 (2015) 1080-1118.

[6] N. Ghaffour, J. Bundschuh, H. Mahmoudi, M.F.A. Goosen, Renewable energy-driven desalination technologies: A comprehensive review on challenges and potential applications of integrated systems, Desalination, 356 (2015) 94-114.

[7] P.K. Smolders and A.C.M. Franken, Terminology for membrane distillation, Desalination, 72 (1989) 249-262.

[8] Alhamadani, Ali & Shukla, Shailendra. (2013). Performance of Single Slope Solar Still with Solar Protected Condenser. Distributed Generation & Alternative Energy Journal. 28. 6-28. 10.1080/21563306.2013.10677548.

[9] Kumar Ashok, Tiwari GN. Use of waste hot water in double slope solar still through heat exchanger. Energy Conversion and Management 1990;30(2):81–9.

[10] K. Sampathkumar, T.V. Arjunan, P. Pitchandi, P. Senthilkumar, Active solar distillation—A detailed review, Renewable and Sustainable Energy Reviews, Volume 14, Issue 6, 2010, Pages 1503-1526.

[11] Tiwari GN, Vimal Dimri, Arvind Chel. Parametric study of an active and passive solar distillation system: energy and exergy analysis. Desalination 2009; 242:1–18.

[12] Zhai, Y., Ma, Y., David, S. N., Zhao, D., Lou, R., Tan, G., Yang, R. & Yin, X. (2017). Scalable manufactured randomized glass-polymer hybrid metamaterial for daytime radiative cooling. Science, 355(6329), 1062-1066.

[13] Lide D R (ed) 2008 CRC Handbook of Chemistry and Physics 88th edn (Boca Raton, FL: CRC Press)

[14] William S. Beichand and Nicholas Turner"Polymer optics: a manufacturer's perspective on the factors that contribute to successful programs", Proc. SPIE 7788, Polymer Optics Design, Fabrication, and Materials, 778805 (12 August 2010);

[15] Dr. Zoran K. Morvay PhD in electrical engineering, Dr. Dušan D. Gvozdenac PhD, "Applied Industrial Energy and Environmental Management" Part 3,toolbox 6. Page (429-230)

[16] Hongfei Zheng, Xiaoyan Zhang, Jing Zhang, Yuyuan Wu. A group of improved heat and mass transfer correlations in solar stills. Energy Conversion and Management 2002;43:2469–78.

[17] Dunkle RV. Solar water distillation, the roof type solar still and a multi effect diffusion still, International developments in heat transfer, ASME Proceedings of International Heat Transfer, University of Colorado. 1961; 5:895–902.

[18] Omar O Badran, Mazen M Abu-Khader. Evaluating thermal performance of a single slope solar still. Heat Mass Transfer 2007; 43:985–95.

[19] Tiwari GN, Tiwari AK. Solar distillation practice for water desalination systems. New Delhi: Anamaya Publishers; 2008.